Short Article

Molecular Cell

Mammalian RAD52 Functions in Break-Induced Replication Repair of Collapsed DNA Replication Forks

Graphical Abstract

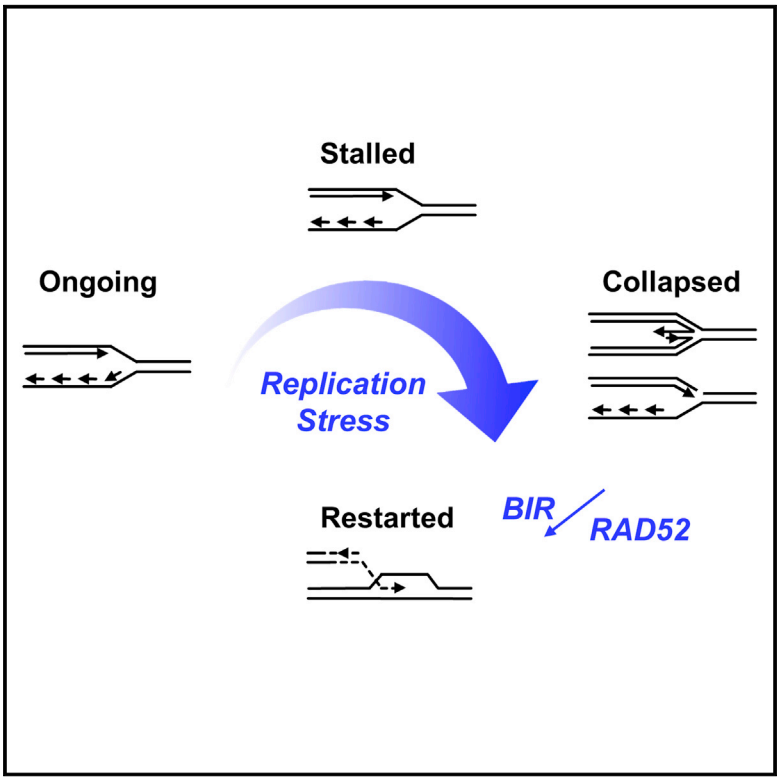

Authors

Sotirios K. Sotiriou, Irene Kamileri, Natalia Lugli, ..., Vassilis G. Gorgoulis, Leonardo Scapozza, Thanos D. Halazonetis

Correspondence

thanos.halazonetis@unige.ch

In Brief

RAD52 is dispensable for life in mammals but is required for double-stranded break (DSB) repair in yeast. Sotiriou et al. now show that mammalian RAD52 plays an important role in response to DNA replication stress by mediating the repair of collapsed DNA replication forks.

Highlights

- Mammalian RAD52 is involved in the oncogene-induced DNA replication stress response
- Mammalian RAD52 functions in the repair of collapsed DNA replication forks
- Rad52 deficiency prolongs the lifespan of *Apc*$^{min/+}$ mice

Sotiriou et al., 2016, Molecular Cell *64*, 1127–1134
December 15, 2016
http://dx.doi.org/10.1016/j.molcel.2016.10.038

Molecular Cell
Short Article

Mammalian RAD52 Functions in Break-Induced Replication Repair of Collapsed DNA Replication Forks

Sotirios K. Sotiriou,[1] Irene Kamileri,[1] Natalia Lugli,[1] Konstantinos Evangelou,[2] Caterina Da-Ré,[1] Florian Huber,[1] Laura Padayachy,[1] Sebastien Tardy,[3] Noemie L. Nicati,[1,3] Samia Barriot,[1] Fena Ochs,[4] Claudia Lukas,[4] Jiri Lukas,[4] Vassilis G. Gorgoulis,[2,5,6] Leonardo Scapozza,[3] and Thanos D. Halazonetis[1,7,*]

[1]Department of Molecular Biology, University of Geneva, 30 Quai Ernest-Ansermet, 1211 Geneva, Switzerland
[2]Department of Histology and Embryology, Medical School, National and Kapodistrian University of Athens, 75 Mikras Asias Street, 11527 Athens, Greece
[3]School of Pharmaceutical Sciences, Department of Pharmaceutical Biochemistry, CMU, University of Geneva and University of Lausanne, Rue Michel-Servet 1, 1211 Geneva, Switzerland
[4]Novo Nordisk Foundation Center for Protein Research, Faculty of Health and Medical Sciences, University of Copenhagen, Blegdamsvej 3B, 2200 Copenhagen, Denmark
[5]Faculty Institute for Cancer Sciences, Manchester Academic Health Sciences Centre, University of Manchester, Manchester M13 9PL, UK
[6]Biomedical Research Foundation, Academy of Athens, 11527 Athens, Greece
[7]Lead Contact
*Correspondence: thanos.halazonetis@unige.ch
http://dx.doi.org/10.1016/j.molcel.2016.10.038

SUMMARY

Human cancers are characterized by the presence of oncogene-induced DNA replication stress (DRS), making them dependent on repair pathways such as break-induced replication (BIR) for damaged DNA replication forks. To better understand BIR, we performed a targeted siRNA screen for genes whose depletion inhibited G1 to S phase progression when oncogenic cyclin E was overexpressed. *RAD52*, a gene dispensable for normal development in mice, was among the top hits. In cells in which fork collapse was induced by oncogenes or chemicals, the Rad52 protein localized to DRS foci. Depletion of Rad52 by siRNA or knockout of the gene by CRISPR/Cas9 compromised restart of collapsed forks and led to DNA damage in cells experiencing DRS. Furthermore, in cancer-prone, heterozygous *APC* mutant mice, homozygous deletion of the *Rad52* gene suppressed tumor growth and prolonged lifespan. We therefore propose that mammalian *RAD52* facilitates repair of collapsed DNA replication forks in cancer cells.

INTRODUCTION

Genomic instability, a key hallmark of cancer, is driven in part by oncogene-induced DNA replication stress (DRS). Specifically, in cancer cells, activated oncogenes induce dissociation of the replication machinery from the DNA fork (fork collapse), formation of DNA double-strand breaks (DSBs), and genomic instability (Gorgoulis et al., 2005; Bartkova et al., 2005, 2006; Bonner et al., 2008; Halazonetis et al., 2008; Negrini et al., 2010; Arlt et al., 2012; Hills and Diffley, 2014; Macheret and Halazonetis, 2015). Prolonged exposure to chemical agents that interfere with DNA replication can also lead to fork collapse (Branzei and Foiani, 2010; Petermann et al., 2010; Yeeles et al., 2013).

Following fork collapse, DNA replication can be completed by repair of the collapsed forks, by incoming replication forks, or by dormant origin firing (Branzei and Foiani, 2010; Blow et al., 2011; Yeeles et al., 2013; Mayle et al., 2015). We previously described break-induced replication (BIR) as a repair pathway for collapsed DNA replication forks in cancer cells (Costantino et al., 2014) and, more recently, the scope of BIR in human cells was expanded to include DNA replication repair in prophase and alternative lengthening of telomeres (Minocherhomji et al., 2015; Dilley et al., 2016; Roumelioti et al., 2016).

BIR has been studied extensively in budding yeast, as a homologous recombination (HR)-based repair pathway for one-ended DNA DSBs (Llorente et al., 2008; Malkova and Ira, 2013; Anand et al., 2013). In BIR, formation of a D loop is followed by establishment of a replication fork. Notably, the D loop moves together with the replication fork, and DNA replication is conservative (Donnianni and Symington, 2013; Saini et al., 2013; Wilson et al., 2013). These unique properties distinguish BIR-initiated forks from origin-initiated forks and suggest the involvement of different proteins at these two types of forks. Indeed, Pol32, a nonessential subunit of budding yeast DNA polymerase delta, is required for BIR, but not for origin-initiated replication (Lydeard et al., 2007). Mammalian PolD3, the ortholog of budding yeast Pol32, is also required for BIR, as is PolD4, another subunit of mammalian DNA polymerase delta that has no apparent ortholog in budding yeast (Costantino et al., 2014; Murga et al., 2016).

In addition to Pol32, BIR in yeast requires Rad52 (Llorente et al., 2008; Payen et al., 2008). However, the role of Rad52 in

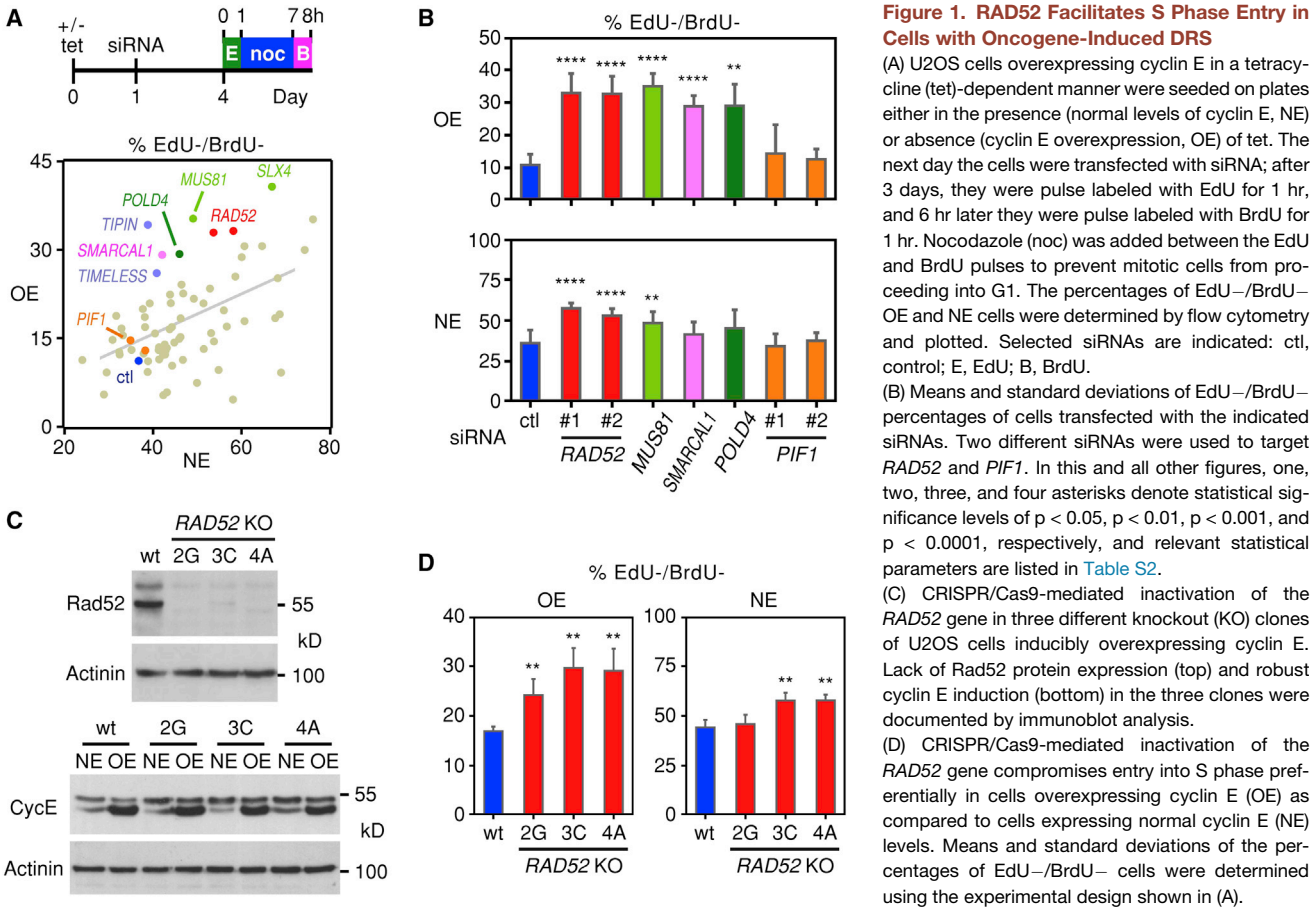

Figure 1. RAD52 Facilitates S Phase Entry in Cells with Oncogene-Induced DRS

(A) U2OS cells overexpressing cyclin E in a tetracycline (tet)-dependent manner were seeded on plates either in the presence (normal levels of cyclin E, NE) or absence (cyclin E overexpression, OE) of tet. The next day the cells were transfected with siRNA; after 3 days, they were pulse labeled with EdU for 1 hr, and 6 hr later they were pulse labeled with BrdU for 1 hr. Nocodazole (noc) was added between the EdU and BrdU pulses to prevent mitotic cells from proceeding into G1. The percentages of EdU−/BrdU− OE and NE cells were determined by flow cytometry and plotted. Selected siRNAs are indicated: ctl, control; E, EdU; B, BrdU.

(B) Means and standard deviations of EdU−/BrdU− percentages of cells transfected with the indicated siRNAs. Two different siRNAs were used to target *RAD52* and *PIF1*. In this and all other figures, one, two, three, and four asterisks denote statistical significance levels of $p < 0.05$, $p < 0.01$, $p < 0.001$, and $p < 0.0001$, respectively, and relevant statistical parameters are listed in Table S2.

(C) CRISPR/Cas9-mediated inactivation of the *RAD52* gene in three different knockout (KO) clones of U2OS cells inducibly overexpressing cyclin E. Lack of Rad52 protein expression (top) and robust cyclin E induction (bottom) in the three clones were documented by immunoblot analysis.

(D) CRISPR/Cas9-mediated inactivation of the *RAD52* gene compromises entry into S phase preferentially in cells overexpressing cyclin E (OE) as compared to cells expressing normal cyclin E (NE) levels. Means and standard deviations of the percentages of EdU−/BrdU− cells were determined using the experimental design shown in (A).

yeast is not specific to BIR; DNA DSB repair by gene conversion (a.k.a. synthesis-dependent strand annealing) and single-strand annealing also require Rad52, and yeast mutants lacking Rad52 are very sensitive to DNA damaging agents (Symington, 2002; Sugawara et al., 2003).

Rad52 is conserved at the amino acid level from yeast to human, but its function is apparently only partially conserved. Thus, human Rad52 retains the strand-annealing activity (Kagawa et al., 2002; Singleton et al., 2002), but gene conversion is mediated primarily by BRCA2 (Prakash et al., 2015). Accordingly, whereas homozygous deletion of the *BRCA2* gene in mice leads to embryonic lethality (Sharan et al., 1997), *RAD52*-knockout mice have a normal lifespan and no major phenotype, raising the question of what the physiological function of mammalian Rad52 is (Rijkers et al., 1998; Yamaguchi-Iwai et al., 1998).

We previously performed an siRNA screen to identify DNA repair genes that are important for cell cycle progression when cyclin E is overexpressed (Costantino et al., 2014). *POLD3* was one of the top hits. Here we performed a more focused screen centering on genes that function in HR, and we identified *RAD52*. Further characterization revealed that *RAD52* has a role in BIR, making it a potential target for the development of cancer-specific therapies.

RESULTS

RAD52 Plays a Role in the Response to Oncogene-Induced DNA Replication Stress

In an effort to identify genes that function in BIR in human cells, we performed an siRNA screen targeting about 70 genes that had previously been linked to DNA DSB repair and HR (Table S1). The requirement of these genes in BIR was examined using U2OS cells that overexpress cyclin E in an inducible manner (Bartkova et al., 2005). In these well-characterized cells, cyclin E overexpression leads to DRS, and the damaged replication forks are repaired to a significant degree by BIR. Thus, when BIR is inhibited—for example, by depleting PolD3—progression through the cell cycle is delayed (Costantino et al., 2014).

To enable monitoring of cell cycle progression, the cells were pulsed consecutively with two thymidine analogs (EdU and BrdU; 1 hr pulse each with the two pulses separated by 6 hr) and then examined by flow cytometry (Figure 1A and Figure S1A). Cells that remained in G1 during the 8 hr period would stain negatively for both EdU and BrdU, whereas cells that transitioned from G1 into S phase would stain negatively for EdU and positively for BrdU. As observed before (Costantino et al., 2014), the fraction of cells that remained in G1 over the 8 hr period decreased when cyclin E was overexpressed (Figure 1A,

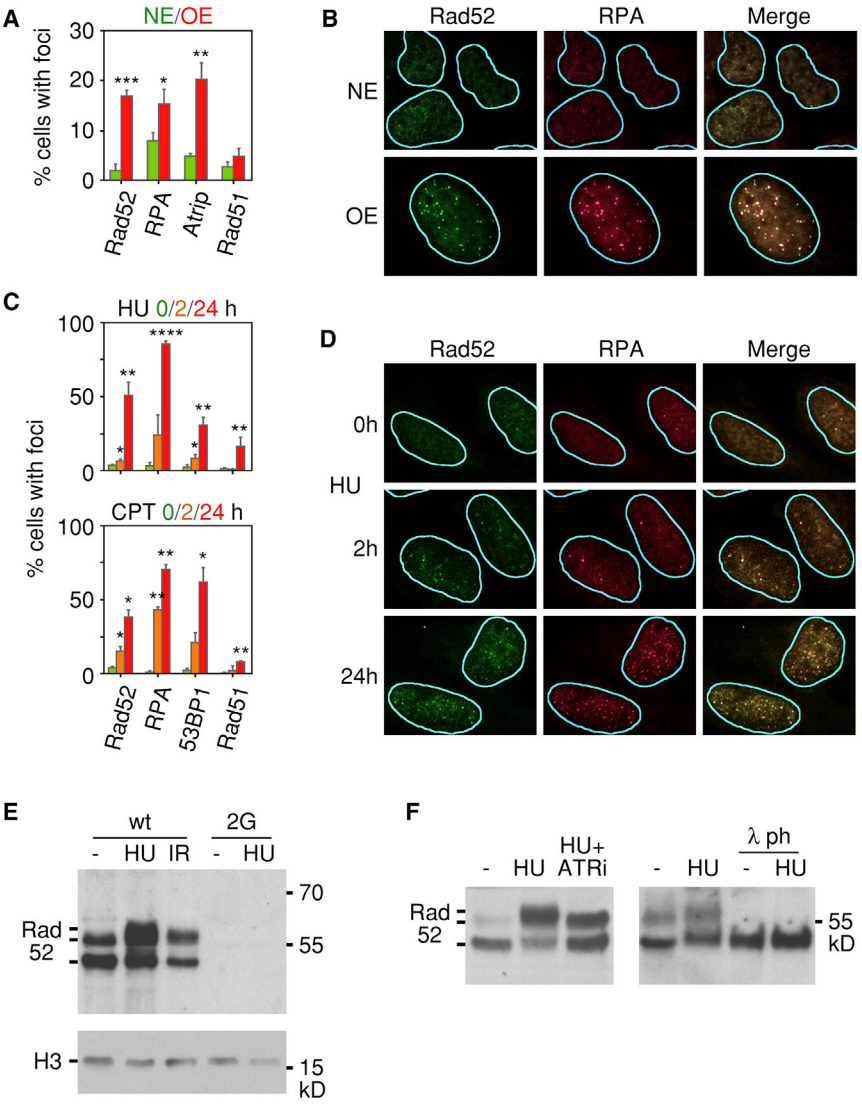

Figure 2. Rad52 Is Recruited to Sites of DRS

(A) Means and standard deviations of the percentages of cells displaying Rad52, RPA, Atrip, or Rad51 foci in the presence of normal (NE) or high (OE) levels of cyclin E. The results are derived from three independent experiments.

(B) Representative immunofluorescence images showing colocalization of Rad52 and RPA foci in cells overexpressing cyclin E (OE).

(C) Means and standard deviations of the percentages of cells displaying Rad52, RPA, 53BP1, or Rad51 foci following treatment with HU or CPT for 0, 2, or 24 hr. The results are derived from three independent experiments.

(D) Representative immunofluorescence images showing colocalization of Rad52 and RPA foci in cells treated with HU for 24 hr.

(E) Posttranslational modifications of chromatin-bound Rad52 in cells treated with hydroxyurea (HU) for 24 hr or exposed to ionizing radiation (IR). U2OS parental cells (WT) and clone 2G with both alleles of *RAD52* inactivated were cultured in the presence of tet to maintain normal levels of cyclin E. The bands corresponding to Rad52 are indicated.

(F) ATR dependence of HU-induced posttranslational modification of chromatin-bound Rad52. U2OS parental cells were cultured in the presence of HU with or without an ATR inhibitor (ATRi) for 24 hr before being harvested. Tet was present in the media to maintain normal levels of cyclin E. Where indicated, the chromatin extracts were treated with lambda phosphatase (λ ph).

control siRNA; NE, normal cyclin E expression; OE, cyclin E overexpression).

Most of the siRNAs tested did not affect the fraction of NE or OE cells that remained in G1 over the 8 hr period (Figure 1A and Table S1). This included two siRNAs that depleted the helicase Pif1, even though in budding yeast Pif1 is required for BIR (Wilson et al., 2013). A small number of siRNAs preferentially enhanced the fraction of cells that remained in G1 when cyclin E was overexpressed. These were the siRNAs targeting *SLX4*, *MUS81*, *SMARCAL1*, *TIPIN*, *TIMELESS*, *POLD4*, and *RAD52* (Figures 1A and 1B). Slx4, an adaptor protein that binds Mus81; Mus81, a nuclease; and SmarcaL1, a helicase, remodel damaged replication forks (Bétous et al., 2012; Pepe and West, 2014; Sarbajna et al., 2014); Tipin and Timeless are part of the replication fork protection complex (Chou and Elledge, 2006; Errico and Costanzo, 2012), while PolD4 functions in BIR (Costantino et al., 2014). We decided to pursue the last hit, Rad52, which is dispensable for normal development in mice, but whose homolog in budding yeast is important for all forms of HR, including BIR.

Using CRISPR/Cas9 (Jinek et al., 2012), we generated *RAD52*-knockout clones in the context of the U2OS cells, in which cyclin E could be inducibly overexpressed. Three independent clones were obtained. Clone 2G contained two mutant alleles, whereas in clones 3C and 4A only one mutant allele was identified (Figure S1B). Clone 3C retained a wild-type (WT) allele, whereas in clones 2G and 4A no WT alleles could be identified. Consistent with the sequencing data, Rad52 protein was undetectable in clones 2G and 4A and barely detectable in clone 3C (Figure 1C). Importantly, all clones retained the capacity to regulate cyclin E levels in a tetracycline (tet)-dependent manner (Figure 1C), and all of them displayed decreased progression from G1 into S phase when cyclin E was overexpressed (Figures 1D and S1C–S1F).

RAD52 Is Recruited to Sites of DRS

We next examined the intracellular localization of Rad52 in cells that were either overexpressing cyclin E or exposed to chemical agents, such as hydroxyurea (HU) and camptothecin (CPT), that induce DRS. In about 20% of cells overexpressing cyclin E for 4 days, endogenous Rad52 localized to DRS foci, as marked by staining for RPA and ATRIP (Figures 2A, 2B, and S2A). Recruitment of Rad52 to DRS foci was also observed in about 50% of the cells exposed to HU for 24 hr but was mostly absent in cells exposed to HU for 2 hr (Figures 2C, 2D, and S2B). These

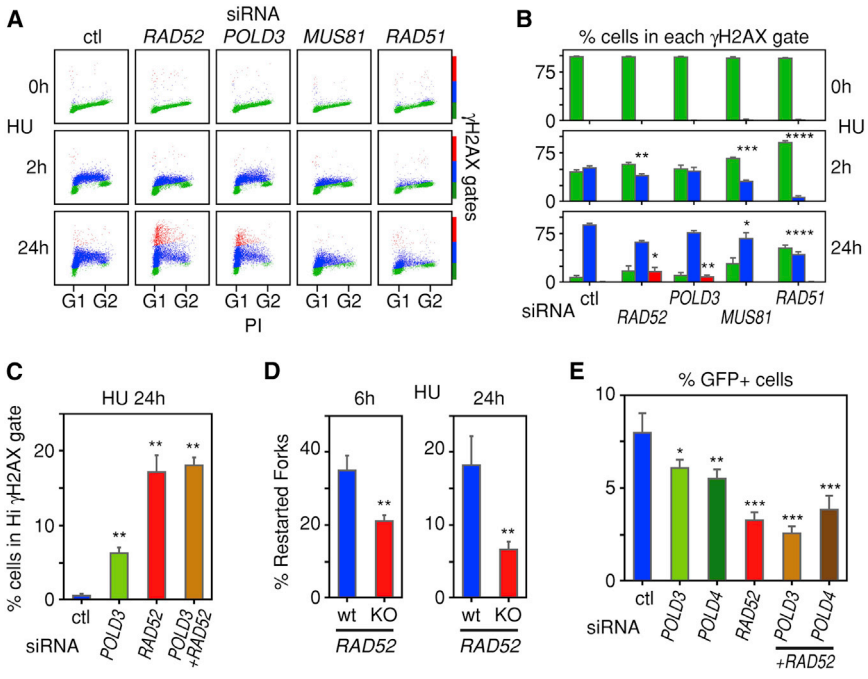

Figure 3. Rad52 Is Required for Fork Restart after Prolonged Exposure of Cells to HU

(A) Rad52 and PolD3 regulate the cellular response to DRS, as ascertained by monitoring histone H2AX phosphorylation (γH2AX) in cells treated with HU for 2 or 24 hr. γH2AX levels were monitored by flow cytometry of cells treated with control (ctl) siRNA or siRNAs targeting *RAD52*, *POLD3*, *MUS81*, or *RAD51*. PI, propidium iodide.

(B) Means and standard deviations of the percentages of cells assigned to the H2AX phosphorylation gates shown in (A), as determined from three independent experiments. Green, blue, and red indicate background, modest, and high H2AX phosphorylation, respectively.

(C) Rad52 and PolD3 regulate the cellular response to DRS epistatically. siRNA-transfected cells were exposed to HU for 24 hr. Means and standard deviations of the percentages of cells assigned to the high (Hi) H2AX phosphorylation gate were derived from two independent experiments.

(D) Fork restart after prolonged exposure of cells to HU is dependent on Rad52. U2OS parental cells (WT) and clone 2G with both alleles of *RAD52* inactivated were cultured in the presence of tet to maintain normal levels of cyclin E. The cells were pulse labeled with CldU for 1 hr, then exposed to HU and a Cdc7 inhibitor for 6 or 24 hr, and finally released into media containing IdU and the Cdc7 inhibitor for 1 hr to allow fork restart. Means and standard deviations of the percentages of restarted forks were derived from three independent DNA fiber experiments.

(E) Effect of depletion of PolD3, PolD4, or Rad52 on repair of DNA DSBs by BIR. Means and standard deviations of the percentages of GFP-positive cells were derived from three independent experiments.

kinetics parallel the known effects of HU on DNA replication forks; short treatment of cells with HU leads to a reduction in the ribonucleotide pools and fork stalling, whereas forks collapse after prolonged exposure to HU (Petermann et al., 2010).

Exposure of cells to CPT, which induces covalent bonding of topoisomerase I to DNA and, subsequently, fork collapse (Pommier, 2006), also led to recruitment of Rad52 to DRS foci; this was evident within 2 hr of exposure in some cells but was much more evident at 24 hr (Figures 2C and S2C). Interestingly, in cells overexpressing cyclin E or exposed to either HU or CPT, Rad51 foci were less prevalent than Rad52 foci (Figures 2A and 2C); however, the functional significance, if any, of this apparent difference remains to be investigated.

Exposure of cells to HU for 24 hr was also associated with posttranslational modifications of the chromatin-bound fraction of Rad52, as detected by immunoblotting, whereas a high dose (9 Gy) of ionizing radiation did not elicit similar modifications (Figure 2E). A subset of the Rad52 posttranslational modifications induced in response to HU were ATR dependent, since they were suppressed when the cells were treated with an ATR inhibitor (Figure 2F). Furthermore, the modifications were sensitive to treatment of the chromatin extracts with lambda phosphatase (Figure 2F). Taken together, these results suggest that ATR phosphorylates Rad52 at sites of DRS.

Enhanced DNA Damage Response following Rad52 Depletion in Cells Treated with HU

If Rad52 is important for BIR, then its depletion should compromise the repair of collapsed forks and lead to a stronger DNA damage response. To explore this possibility, we depleted Rad52 by siRNA and monitored H2AX phosphorylation both 2 and 24 hr after adding HU to the cells. At the 24 hr time point, the majority of the replication forks were collapsed, whereas at early time points, a large fraction of the forks are stalled and can resume replication upon HU withdrawal (Figure S3A). The effects of PolD3, Mus81, and Rad51 depletion on H2AX phosphorylation were also examined (Figure S3B).

Two hours after exposure of the cells to HU, γH2AX levels increased modestly and equally in the control, Rad52-, PolD3-, and Mus81-depleted cells (Figures 3A and 3B). After 24 hr exposure to HU, γH2AX phosphorylation levels increased further, but the increase was much stronger in the cells depleted for Rad52 or PolD3 (Figures 3A and 3B). Codepleting Rad52 and PolD3 had the same effect as depleting only Rad52 (Figure 3C). These results are consistent with Rad52 and PolD3 functioning epistatically in repair of collapsed, but not stalled, replication forks. Interestingly, depletion of Rad51 suppressed γH2AX phosphorylation when compared to control siRNA-treated cells at both the 2 and 24 hr time points, an observation that merits further study (Figures 3A and 3B).

Rad52 Facilitates Restart of Collapsed Replication Forks

To examine whether Rad52 facilitates restart of replication after fork collapse, we performed DNA fiber analysis of cells exposed to HU for 6 or 24 hr. However, we were concerned that new origin firing near a collapsed fork might be misinterpreted as fork restart if replication from the new origin proceeded all the way

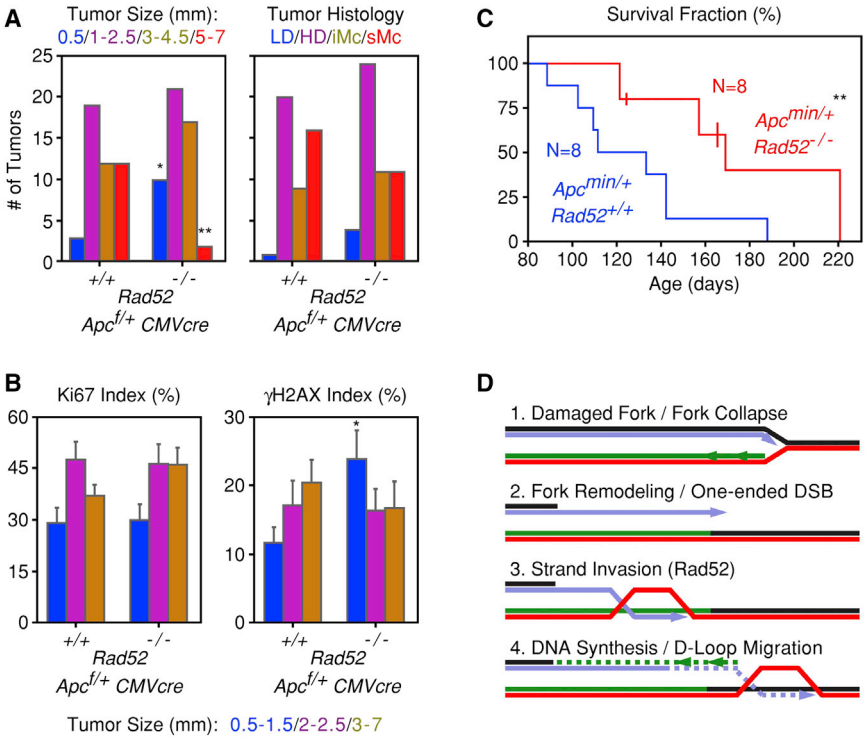

Figure 4. Rad52 Deficiency Restrains Tumor Growth and Prolongs Survival of Mice with *APC* Mutations

(A) Comparison of tumors present in the intestines of *Rad52*$^{+/+}$;*Apc*$^{f/+}$;*CMVcre* (N = 6) and *Rad52*$^{-/-}$;*Apc*$^{f/+}$;*CMVcre* (N = 6) mice. Tumors were stratified according to size (in mm) or according to histopathological criteria: LD, low-grade dysplasia; HD, high-grade dysplasia; iMc, intramucosal; and sMc, submucosal.

(B) Proliferation (Ki67) and DNA damage (γH2AX) indices of the tumors present in the intestines of the *Rad52*$^{+/+}$;*Apc*$^{f/+}$;*CMVcre* and *Rad52*$^{-/-}$;*Apc*$^{f/+}$;*CMVcre* mice. Means and standard deviations of the indices were calculated after stratifying the tumors into three groups according to size.

(C) Survival fractions of *Rad52*$^{+/+}$;*Apc*$^{min/+}$ (N = 8) and *Rad52*$^{-/-}$;*Apc*$^{min/+}$ (N = 8) mice. Three of the *Rad52*$^{-/-}$;*Apc*$^{min/+}$ mice, indicated by vertical lines in the graph, had not died at the time the data were recorded and were considered censored for the statistical analysis.

(D) Proposed model for the role of Rad52 in BIR.

to the collapsed fork. We therefore performed the assay in the presence of a Cdc7 inhibitor that does not inhibit transcription (Menichincheri et al., 2010; Montagnoli et al., 2010a, 2010b) after demonstrating that this inhibitor effectively suppressed new origin firing in cells released from a 24 hr HU replication block (Figures S3A and S3C).

To monitor fork restart, the cells were incubated with CldU for 1 hr, then incubated with HU for 6 or 24 hr in the presence of the Cdc7 inhibitor; finally, after release from the HU block, the cells were incubated with IdU for 1 hr again in the presence of the Cdc7 inhibitor to prevent new origin firing. The 1 hr IdU incubation period was found to be sufficient to observe restart of replication. In the parental U2OS cells, replication restart was observed after exposure to HU for both 6 and 24 hr, although this was the case to a greater extent for the shorter incubation period (Figure 3D). In the *RAD52*-knockout clone, replication restart was significantly reduced, especially when the cells were exposed to HU for 24 hr (Figures 3D and S3D). Since the Cdc7 inhibitor prevented new origin firing, these results suggest that repair and restart of collapsed forks was Rad52 dependent.

Rad52 Enhances the Efficiency of BIR

To further monitor the function of Rad52 in BIR, we employed a green fluorescent protein (GFP)-based reporter assay in which BIR-mediated repair of DNA DSBs induced by the endonuclease I-SceI leads to GFP fluorescence (Costantino et al., 2014). Since the initial description of this assay, we have generated a new, stably transfected cell clone expressing the GFP reporter plasmid that provides a better signal-to-noise ratio than the original clone. Depletion of Rad52 by siRNA in the new clone led to a significant suppression of GFP fluorescence, consistent with Rad52 functioning in BIR (Figure 3E). Depletion of PolD3 and PolD4 also suppressed BIR in this system, although not as efficiently as Rad52. Interestingly, codepletion of Rad52 and PolD3 or Rad52 and PolD4 suppressed BIR, as efficiently as depletion of Rad52 alone, further suggesting that PolD3, PolD4 and Rad52 function epistatically (Figure 3E).

Rad52 Deletion Restrains Oncogenic Progression in Mice

Since BIR repairs collapsed forks in cells with oncogene-induced DRS, its deletion should curtail cancer development and/or progression. First, we examined tumor formation in *APC*$^{flox/+}$ mice rendered heterozygous for *APC* by constitutively expressing the Cre recombinase under the control of a CMV promoter and enhancer. In these mice, the entire coding sequence of the mutant *APC* allele is deleted by the Cre recombinase (Cheung et al., 2010). In regard to *Rad52*, the mice either had two WT *Rad52* alleles (*Rad52*$^{+/+}$) or were homozygous for deletion of the *Rad52* gene (*Rad52*$^{-/-}$). At 8 months of age, the mice, while still having no overt signs of disease, were sacrificed, and the presence of tumors in the entire small intestine was scored by histology. Deletion of *Rad52* did not affect the number of observed tumors (a total of 46 versus 50 tumors in six *Rad52*$^{+/+}$ and six *Rad52*$^{-/-}$ mice, respectively), but resulted in smaller tumor sizes (Figure 4A). Deletion of *Rad52* also resulted in an increase in the fraction of tumor cells scoring positive for phosphorylated H2AX, consistent with an inability to repair collapsed replication forks; however, this difference was only evident in the early stages of tumor development, when tumors were less than 1.5 mm in diameter (Figures 4B and S4).

The effect of *Rad52* on cancer progression was further examined in APC^{min} heterozygous mice. In a WT *Rad52* background, the lifespan of these mice is significantly shorter than that of mice bearing the APC^{flox} allele described above (Moser et al., 1990). We therefore used the APC^{min} model to ascertain whether loss of *Rad52* affected survival. Indeed, lifespan of the APC^{min} heterozygous mice was significantly extended from a mean of 127 days for the $Rad52^{+/+}$ mice to 178 days for the $Rad52^{-/-}$ mice (Figure 4C).

DISCUSSION

The function of Rad52 in DNA repair is well established in yeast, but less well defined in higher eukaryotes and mammals (Symington, 2002). In fact, mice with homozygous deletion of the *Rad52* gene are viable and have no obvious phenotype (Rijkers et al., 1998). This could indicate that Rad52 serves a backup function that is relevant only when the primary DNA DSB repair pathways are inactivated or overwhelmed by excessive DNA damage. Supporting this model, depletion of *Rad52* is synthetic lethal with BRCA2 deficiency in human cell lines (Feng et al., 2011; Lok and Powell, 2012). Also, cells rely on Rad52 for repair when extensive DNA damage overwhelms the repair capacities of BRCA1 and 53BP1 (Ochs et al., 2016). However, the findings reported here suggest that Rad52 has more than a backup role in DNA repair. Specifically, we propose that Rad52 has a key role in BIR repair of collapsed DNA replication forks (Figure 4D).

Several observations support a role of Rad52 in BIR. Endogenous Rad52 localized to sites of DRS in cells with collapsed DNA replication forks, depletion of Rad52 led to increased levels of DNA damage in cells exposed to HU for 24 hr, DNA replication restart from collapsed forks was dependent on Rad52, and Rad52 depletion suppressed repair of DNA DSBs by BIR in a GFP-based reporter assay. Together with the known biochemical function of mammalian Rad52 in strand annealing (Kagawa et al., 2002; Singleton et al., 2002), these results argue that strand invasion by Rad52 leads to DNA structures that are conducive to initiation of DNA replication after fork collapse.

In yeast, Rad52 is important for Rad51-dependent and Rad51-independent forms of HR. Whereas repair of DNA DSBs by gene conversion in yeast is Rad51 dependent, BIR can be Rad51 independent (Ira and Haber, 2002; Payen et al., 2008). In this case, the strand annealing activity of Rad52 is important, and indeed, it is easy to envision the presence of single-stranded template DNA to which the invading strand can anneal at collapsed DNA replication forks. By analogy, mammalian Rad52, with or without Rad51, may be involved in the strand-invasion step of BIR, as is the case for its ortholog in yeast (Llorente et al., 2008; Malkova and Ira, 2013; Anand et al., 2013).

A role for Rad52 in BIR can explain why its depletion in cells with DRS leads to increased DNA damage (Wray et al., 2008; Murfuni et al., 2013; Galanos et al., 2016; Figures 3A and 3B), why the *RAD52* gene is amplified in human cancers, and why its inactivation curtails cancer development (Treuner et al., 2004; Cramer-Morales et al., 2013; Lieberman et al., 2016; Figure 4). BIR also mediates DNA repair synthesis in mitosis (Minocherhomji et al., 2015), and it is noteworthy that Rad52 is essential also in this context (Bhowmick et al., 2016).

EXPERIMENTAL PROCEDURES

siRNA Screen and Generation of RAD52-Deficient Clones

For the siRNA screen, U2OS cells engineered to overexpress cyclin E in an inducible (tet-off system) manner (U2OS-CycE cells) were plated in the presence or absence of tet, and the next day they were transfected with siRNA. Then, 3 days later, the cells were pulsed for 1 hr with EdU; 6 hr after that, they were pulsed for 1 hr with BrdU and then processed for flow cytometry as described (Costantino et al., 2014). To generate *RAD52*-knockout U2OS-CycE cells, two CRISPR/Cas9 constructs targeting exons 3 and 9 of the human *RAD52* gene, respectively, were used. After transfection, single clones were expanded and characterized by DNA sequencing of the targeted alleles and by immunoblotting for Rad52 protein.

Immunofluorescence and Flow Cytometry Analysis of the γH2AX Content

Either U2OS-CycE cells grown in the presence or absence of tet for 4 days or U2OS parental cells treated with 2 mM HU or 2 μM CPT were processed for immunofluorescence, as described (Costantino et al., 2014). To monitor γH2AX levels by flow cytometry, U2OS cells transfected with the indicated siRNAs were treated with 2 mM HU for 0, 2, or 24 hr; fixed in 70% ice-cold ethanol; and stained using the FlowCellect Histone H2AX Phosphorylation Assay Kit (Millipore).

DNA Fiber Analysis

U2OS cells were pulse labeled with CldU for 1 hr, then treated with 2 mM HU and Cdc7 inhibitor for 6 or 24 hr, and finally pulse labeled with IdU for 1 hr in the presence of the Cdc7 inhibitor. DNA fibers were spread on APS-coated coverslips and visualized using primary antibodies recognizing CldU or IdU.

See the Supplemental Information for a full list of antibodies as well as a full list and detailed description of the methods used in this study.

SUPPLEMENTAL INFORMATION

Supplemental Information includes Supplemental Experimental Procedures, four figures, and four tables and can be found with this article online at http://dx.doi.org/10.1016/j.molcel.2016.10.038.

AUTHOR CONTRIBUTIONS

S.K.S. and T.D.H. conceived the study. S.K.S., I.K., N.L., K.E., C.D.-R., F.H., L.P., N.L.N., and S.B. planned and performed the experiments. L.S. planned the chemical synthesis, and S.T. synthesized the Cdc7 inhibitor. S.K.S., I.K., N.L., K.E., C.D.-R., F.H., L.P., S.T., N.L.N., S.B., F.O., C.L., J.L., V.G.G., L.S., and T.D.H. proposed experiments, discussed the results, and contributed to the writing of the manuscript.

ACKNOWLEDGMENTS

The authors thank Ian Hickson for sharing unpublished results, Massimo Lopes for advice on the DNA-fiber-spreading protocol, and Samuel Espy for help on the chemical synthesis of the Cdc7 inhibitor. This study was supported by funds from the Swiss National Science Foundation (SNF 160322) and the European Commission (ERC ONIDDAC) to T.D.H., funds from the Swiss National Science Foundation (CRSI33_130016) to L.S., funds from the Novo Nordisk Foundation (NNF 14CC0001) and Danish Cancer Society (R72-A4436) to C.L. and J.L., and funds from the Greek GSRT Program (Aristeia II-3020) to V.G.G., as well as an EMBO long-term postdoctoral fellowship to I.K.

Received: July 13, 2016
Revised: October 8, 2016
Accepted: October 28, 2016
Published: December 15, 2016

REFERENCES

Anand, R.P., Lovett, S.T., and Haber, J.E. (2013). Break-induced DNA replication. Cold Spring Harb. Perspect. Biol. *5*, a010397.

Arlt, M.F., Wilson, T.E., and Glover, T.W. (2012). Replication stress and mechanisms of CNV formation. Curr. Opin. Genet. Dev. *22*, 204–210.

Bartkova, J., Horejsí, Z., Koed, K., Krämer, A., Tort, F., Zieger, K., Guldberg, P., Sehested, M., Nesland, J.M., Lukas, C., et al. (2005). DNA damage response as a candidate anti-cancer barrier in early human tumorigenesis. Nature *434*, 864–870.

Bartkova, J., Rezaei, N., Liontos, M., Karakaidos, P., Kletsas, D., Issaeva, N., Vassiliou, L.V., Kolettas, E., Niforou, K., Zoumpourlis, V.C., et al. (2006). Oncogene-induced senescence is part of the tumorigenesis barrier imposed by DNA damage checkpoints. Nature *444*, 633–637.

Bétous, R., Mason, A.C., Rambo, R.P., Bansbach, C.E., Badu-Nkansah, A., Sirbu, B.M., Eichman, B.F., and Cortez, D. (2012). SMARCAL1 catalyzes fork regression and Holliday junction migration to maintain genome stability during DNA replication. Genes Dev. *26*, 151–162.

Bhowmick, R., Minocherhomji, S., and Hickson, I.D. (2016). RAD52 facilitates mitotic DNA synthesis following replication stress. Mol. Cell *64*, this issue, 1117–1126.

Blow, J.J., Ge, X.Q., and Jackson, D.A. (2011). How dormant origins promote complete genome replication. Trends Biochem. Sci. *36*, 405–414.

Bonner, W.M., Redon, C.E., Dickey, J.S., Nakamura, A.J., Sedelnikova, O.A., Solier, S., and Pommier, Y. (2008). GammaH2AX and cancer. Nat. Rev. Cancer *8*, 957–967.

Branzei, D., and Foiani, M. (2010). Maintaining genome stability at the replication fork. Nat. Rev. Mol. Cell Biol. *11*, 208–219.

Cheung, A.F., Carter, A.M., Kostova, K.K., Woodruff, J.F., Crowley, D., Bronson, R.T., Haigis, K.M., and Jacks, T. (2010). Complete deletion of Apc results in severe polyposis in mice. Oncogene *29*, 1857–1864.

Chou, D.M., and Elledge, S.J. (2006). Tipin and Timeless form a mutually protective complex required for genotoxic stress resistance and checkpoint function. Proc. Natl. Acad. Sci. USA *103*, 18143–18147.

Costantino, L., Sotiriou, S.K., Rantala, J.K., Magin, S., Mladenov, E., Helleday, T., Haber, J.E., Iliakis, G., Kallioniemi, O.P., and Halazonetis, T.D. (2014). Break-induced replication repair of damaged forks induces genomic duplications in human cells. Science *343*, 88–91.

Cramer-Morales, K., Nieborowska-Skorska, M., Scheibner, K., Padget, M., Irvine, D.A., Sliwinski, T., Haas, K., Lee, J., Geng, H., Roy, D., et al. (2013). Personalized synthetic lethality induced by targeting RAD52 in leukemias identified by gene mutation and expression profile. Blood *122*, 1293–1304.

Dilley, R.L., Verma, P., Cho, N.W., Winters, H.D., Wondisford, A.R., and Greenberg, R.A. (2016). Break-induced telomere synthesis underlies alternative telomere maintenance. Nature *539*, 54–58.

Donnianni, R.A., and Symington, L.S. (2013). Break-induced replication occurs by conservative DNA synthesis. Proc. Natl. Acad. Sci. USA *110*, 13475–13480.

Errico, A., and Costanzo, V. (2012). Mechanisms of replication fork protection: a safeguard for genome stability. Crit. Rev. Biochem. Mol. Biol. *47*, 222–235.

Feng, Z., Scott, S.P., Bussen, W., Sharma, G.G., Guo, G., Pandita, T.K., and Powell, S.N. (2011). Rad52 inactivation is synthetically lethal with BRCA2 deficiency. Proc. Natl. Acad. Sci. USA *108*, 686–691.

Galanos, P., Vougas, K., Walter, D., Polyzos, A., Maya-Mendoza, A., Haagensen, E.J., Kokkalis, A., Roumelioti, F.M., Gagos, S., Tzetis, M., et al. (2016). Chronic p53-independent p21 expression causes genomic instability by deregulating replication licensing. Nat. Cell Biol. *18*, 777–789.

Gorgoulis, V.G., Vassiliou, L.V., Karakaidos, P., Zacharatos, P., Kotsinas, A., Liloglou, T., Venere, M., Ditullio, R.A., Jr., Kastrinakis, N.G., Levy, B., et al. (2005). Activation of the DNA damage checkpoint and genomic instability in human precancerous lesions. Nature *434*, 907–913.

Halazonetis, T.D., Gorgoulis, V.G., and Bartek, J. (2008). An oncogene-induced DNA damage model for cancer development. Science *319*, 1352–1355.

Hills, S.A., and Diffley, J.F. (2014). DNA replication and oncogene-induced replicative stress. Curr. Biol. *24*, R435–R444.

Ira, G., and Haber, J.E. (2002). Characterization of RAD51-independent break-induced replication that acts preferentially with short homologous sequences. Mol. Cell. Biol. *22*, 6384–6392.

Jinek, M., Chylinski, K., Fonfara, I., Hauer, M., Doudna, J.A., and Charpentier, E. (2012). A programmable dual-RNA-guided DNA endonuclease in adaptive bacterial immunity. Science *337*, 816–821.

Kagawa, W., Kurumizaka, H., Ishitani, R., Fukai, S., Nureki, O., Shibata, T., and Yokoyama, S. (2002). Crystal structure of the homologous-pairing domain from the human Rad52 recombinase in the undecameric form. Mol. Cell *10*, 359–371.

Lieberman, R., Xiong, D., James, M., Han, Y., Amos, C.I., Wang, L., and You, M. (2016). Functional characterization of RAD52 as a lung cancer susceptibility gene in the 12p13.33 locus. Mol. Carcinog. *55*, 953–963.

Llorente, B., Smith, C.E., and Symington, L.S. (2008). Break-induced replication: what is it and what is it for? Cell Cycle *7*, 859–864.

Lok, B.H., and Powell, S.N. (2012). Molecular pathways: understanding the role of Rad52 in homologous recombination for therapeutic advancement. Clin. Cancer Res. *18*, 6400–6406.

Lydeard, J.R., Jain, S., Yamaguchi, M., and Haber, J.E. (2007). Break-induced replication and telomerase-independent telomere maintenance require Pol32. Nature *448*, 820–823.

Macheret, M., and Halazonetis, T.D. (2015). DNA replication stress as a hallmark of cancer. Annu. Rev. Pathol. *10*, 425–448.

Malkova, A., and Ira, G. (2013). Break-induced replication: functions and molecular mechanism. Curr. Opin. Genet. Dev. *23*, 271–279.

Mayle, R., Campbell, I.M., Beck, C.R., Yu, Y., Wilson, M., Shaw, C.A., Bjergbaek, L., Lupski, J.R., and Ira, G. (2015). DNA REPAIR. Mus81 and converging forks limit the mutagenicity of replication fork breakage. Science *349*, 742–747.

Menichincheri, M., Albanese, C., Alli, C., Ballinari, D., Bargiotti, A., Caldarelli, M., Ciavolella, A., Cirla, A., Colombo, M., Colotta, F., et al. (2010). Cdc7 kinase inhibitors: 5-heteroaryl-3-carboxamido-2-aryl pyrroles as potential antitumor agents. 1. Lead finding. J. Med. Chem. *53*, 7296–7315.

Minocherhomji, S., Ying, S., Bjerregaard, V.A., Bursomanno, S., Aleliunaite, A., Wu, W., Mankouri, H.W., Shen, H., Liu, Y., and Hickson, I.D. (2015). Replication stress activates DNA repair synthesis in mitosis. Nature *528*, 286–290.

Montagnoli, A., Moll, J., and Colotta, F. (2010a). Targeting cell division cycle 7 kinase: a new approach for cancer therapy. Clin. Cancer Res. *16*, 4503–4508.

Montagnoli, A., Ballinari, D., Ciavolella, A., Rainoldi, S., Menichincheri, M., Pesenti, E., Galvani, A., Isacchi, A., and Moll, J. (2010b). Activity of the Cdc7 inhibitor NMS-1116354 as single agent and in combination in breast cancer models. EJC Suppl. *8*, 49.

Moser, A.R., Pitot, H.C., and Dove, W.F. (1990). A dominant mutation that predisposes to multiple intestinal neoplasia in the mouse. Science *247*, 322–324.

Murfuni, I., Basile, G., Subramanyam, S., Malacaria, E., Bignami, M., Spies, M., Franchitto, A., and Pichierri, P. (2013). Survival of the replication checkpoint deficient cells requires MUS81-RAD52 function. PLoS Genet. *9*, e1003910.

Murga, M., Lecona, E., Kamileri, I., Díaz, M., Lugli, N., Sotiriou, S.K., Anton, M.E., Méndez, J., Halazonetis, T.D., and Fernandez-Capetillo, O. (2016). POLD3 is haploinsufficient for DNA replication in mice. Mol. Cell *63*, 877–883.

Negrini, S., Gorgoulis, V.G., and Halazonetis, T.D. (2010). Genomic instability—an evolving hallmark of cancer. Nat. Rev. Mol. Cell Biol. *11*, 220–228.

Ochs, F., Somyajit, K., Altmeyer, M., Rask, M.B., Lukas, J., and Lukas, C. (2016). 53BP1 fosters fidelity of homology-directed DNA repair. Nat. Struct. Mol. Biol. *23*, 714–721.

Payen, C., Koszul, R., Dujon, B., and Fischer, G. (2008). Segmental duplications arise from Pol32-dependent repair of broken forks through two alternative replication-based mechanisms. PLoS Genet. *4*, e1000175.

Pepe, A., and West, S.C. (2014). MUS81-EME2 promotes replication fork restart. Cell Rep. *7*, 1048–1055.

Petermann, E., Orta, M.L., Issaeva, N., Schultz, N., and Helleday, T. (2010). Hydroxyurea-stalled replication forks become progressively inactivated and require two different RAD51-mediated pathways for restart and repair. Mol. Cell *37*, 492–502.

Pommier, Y. (2006). Topoisomerase I inhibitors: camptothecins and beyond. Nat. Rev. Cancer *6*, 789–802.

Prakash, R., Zhang, Y., Feng, W., and Jasin, M. (2015). Homologous recombination and human health: the roles of BRCA1, BRCA2, and associated proteins. Cold Spring Harb. Perspect. Biol. *7*, a016600.

Rijkers, T., Van Den Ouweland, J., Morolli, B., Rolink, A.G., Baarends, W.M., Van Sloun, P.P., Lohman, P.H., and Pastink, A. (1998). Targeted inactivation of mouse RAD52 reduces homologous recombination but not resistance to ionizing radiation. Mol. Cell. Biol. *18*, 6423–6429.

Roumelioti, F.M., Sotiriou, S.K., Katsini, V., Chiourea, M., Halazonetis, T.D., and Gagos, S. (2016). Alternative lengthening of human telomeres is a conservative DNA replication process with features of break-induced replication. EMBO Rep. e201643169.

Saini, N., Ramakrishnan, S., Elango, R., Ayyar, S., Zhang, Y., Deem, A., Ira, G., Haber, J.E., Lobachev, K.S., and Malkova, A. (2013). Migrating bubble during break-induced replication drives conservative DNA synthesis. Nature *502*, 389–392.

Sarbajna, S., Davies, D., and West, S.C. (2014). Roles of SLX1-SLX4, MUS81-EME1, and GEN1 in avoiding genome instability and mitotic catastrophe. Genes Dev. *28*, 1124–1136.

Sharan, S.K., Morimatsu, M., Albrecht, U., Lim, D.S., Regel, E., Dinh, C., Sands, A., Eichele, G., Hasty, P., and Bradley, A. (1997). Embryonic lethality and radiation hypersensitivity mediated by Rad51 in mice lacking Brca2. Nature *386*, 804–810.

Singleton, M.R., Wentzell, L.M., Liu, Y., West, S.C., and Wigley, D.B. (2002). Structure of the single-strand annealing domain of human RAD52 protein. Proc. Natl. Acad. Sci. USA *99*, 13492–13497.

Sugawara, N., Wang, X., and Haber, J.E. (2003). In vivo roles of Rad52, Rad54, and Rad55 proteins in Rad51-mediated recombination. Mol. Cell *12*, 209–219.

Symington, L.S. (2002). Role of RAD52 epistasis group genes in homologous recombination and double-strand break repair. Microbiol. Mol. Biol. Rev. *66*, 630–670.

Treuner, K., Helton, R., and Barlow, C. (2004). Loss of Rad52 partially rescues tumorigenesis and T-cell maturation in Atm-deficient mice. Oncogene *23*, 4655–4661.

Wilson, M.A., Kwon, Y., Xu, Y., Chung, W.H., Chi, P., Niu, H., Mayle, R., Chen, X., Malkova, A., Sung, P., and Ira, G. (2013). Pif1 helicase and Polδ promote recombination-coupled DNA synthesis via bubble migration. Nature *502*, 393–396.

Wray, J., Liu, J., Nickoloff, J.A., and Shen, Z. (2008). Distinct RAD51 associations with RAD52 and BCCIP in response to DNA damage and replication stress. Cancer Res. *68*, 2699–2707.

Yamaguchi-Iwai, Y., Sonoda, E., Buerstedde, J.M., Bezzubova, O., Morrison, C., Takata, M., Shinohara, A., and Takeda, S. (1998). Homologous recombination, but not DNA repair, is reduced in vertebrate cells deficient in RAD52. Mol. Cell. Biol. *18*, 6430–6435.

Yeeles, J.T., Poli, J., Marians, K.J., and Pasero, P. (2013). Rescuing stalled or damaged replication forks. Cold Spring Harb. Perspect. Biol. *5*, a012815.

Molecular Cell, Volume *64*

Supplemental Information

Mammalian RAD52 Functions in Break-Induced Replication Repair of Collapsed DNA Replication Forks

Sotirios K. Sotiriou, Irene Kamileri, Natalia Lugli, Konstantinos Evangelou, Caterina Da-Ré, Florian Huber, Laura Padayachy, Sebastien Tardy, Noemie L. Nicati, Samia Barriot, Fena Ochs, Claudia Lukas, Jiri Lukas, Vassilis G. Gorgoulis, Leonardo Scapozza, and Thanos D. Halazonetis

This PDF file contains:

Figures S1 to S4
Supplemental Figure Legends
Tables S1 to S4
Supplemental Experimental Procedures
Supplemental References

Fig. S1

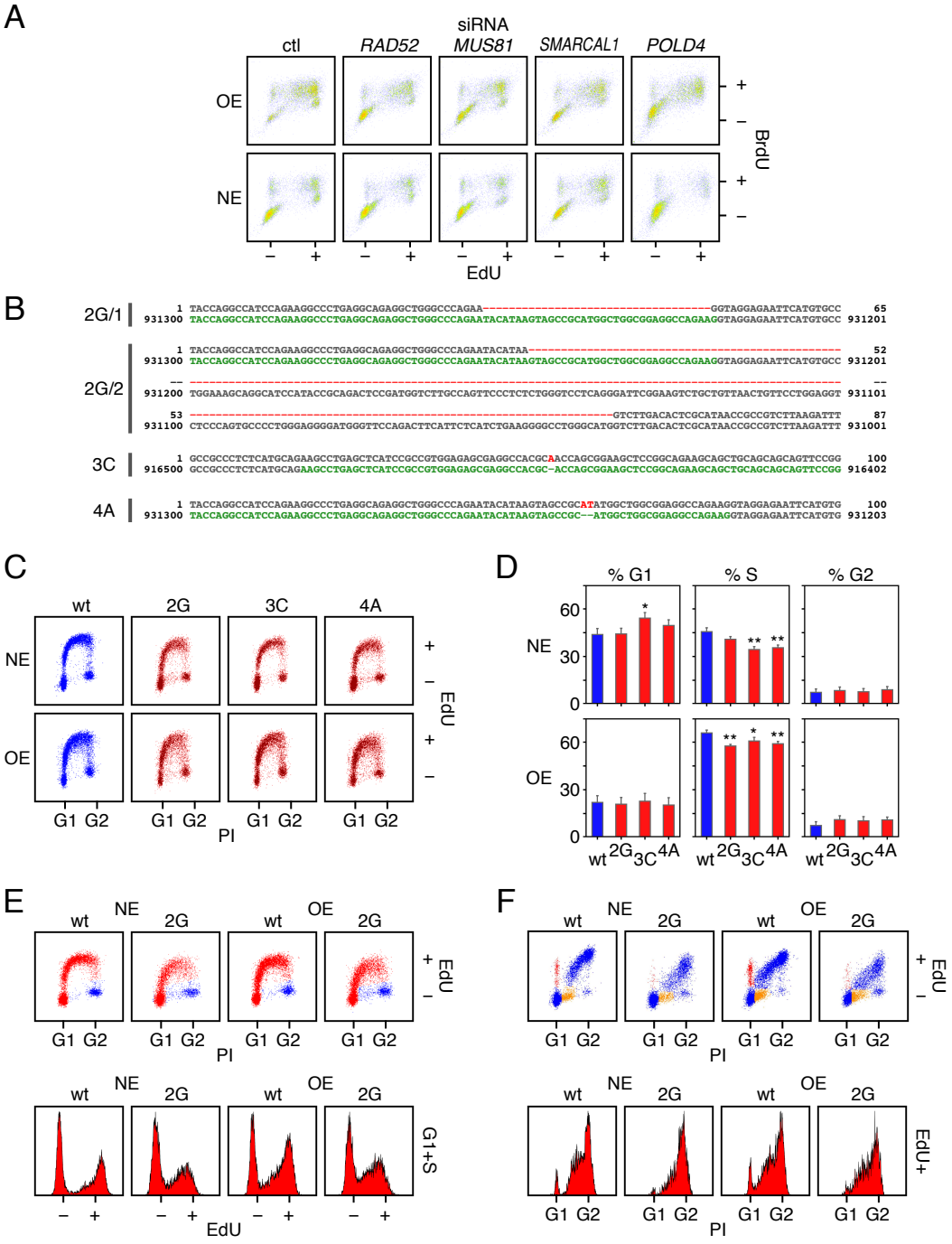
A
siRNA
ctl
RAD52
MUS81
SMARCAL1
POLD4
OE
NE
BrdU
EdU
B
2G/1
2G/2
3C
4A
C
wt
2G
3C
4A
NE
OE
EdU
G1 G2
PI
D
% G1
% S
% G2
E
F
G1+S
EdU+

Fig. S2

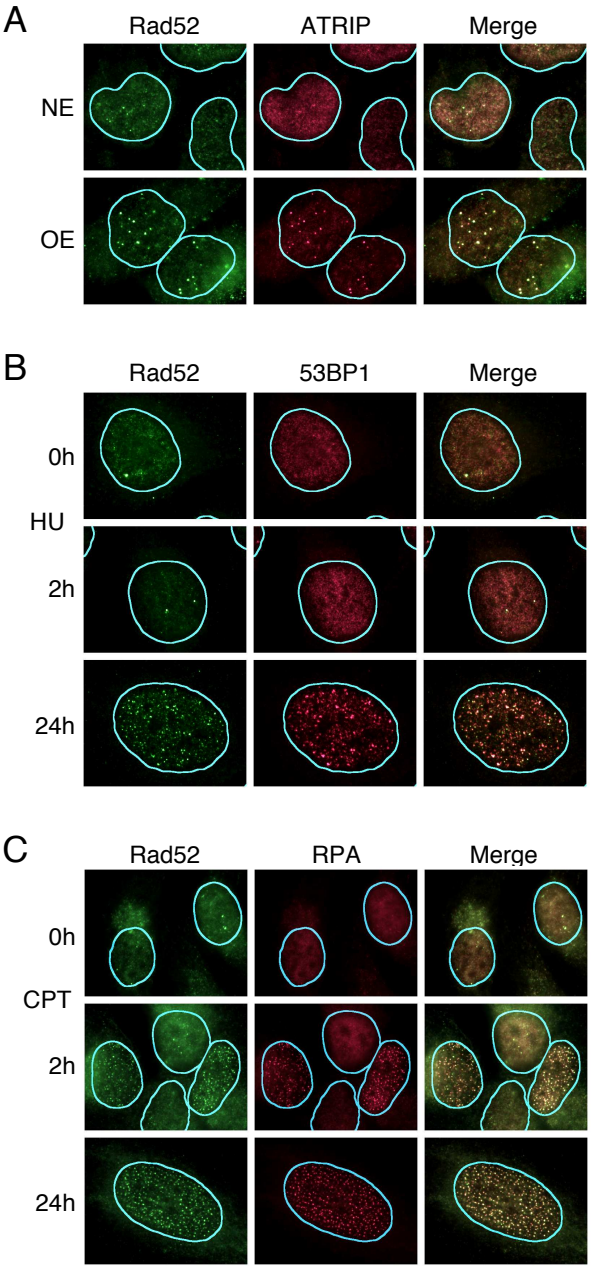
A
Rad52
ATRIP
Merge
NE
OE
B
Rad52
53BP1
Merge
0h
HU
2h
24h
C
Rad52
RPA
Merge
0h
CPT
2h
24h

Fig. S3

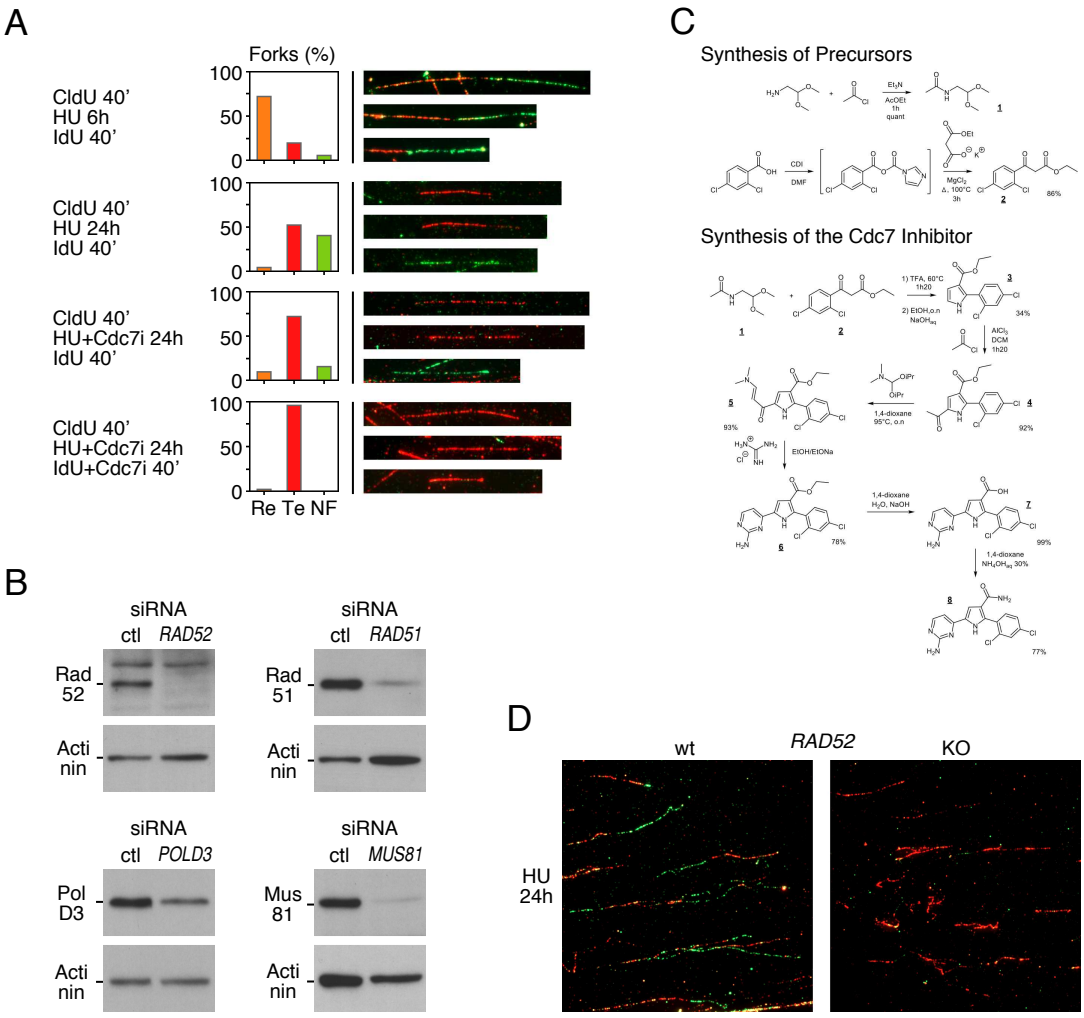
A
Forks (%)
CldU 40'
HU 6h
IdU 40'
CldU 40'
HU 24h
IdU 40'
CldU 40'
HU+Cdc7i 24h
IdU 40'
CldU 40'
HU+Cdc7i 24h
IdU+Cdc7i 40'
100
50
0
Re Te NF
B
siRNA
ctl RAD52
Rad 52
Acti nin
siRNA
ctl RAD51
Rad 51
Acti nin
siRNA
ctl POLD3
Pol D3
Acti nin
siRNA
ctl MUS81
Mus 81
Acti nin
C
Synthesis of Precursors
Synthesis of the Cdc7 Inhibitor
D
wt
RAD52
KO
HU 24h

Fig. S4

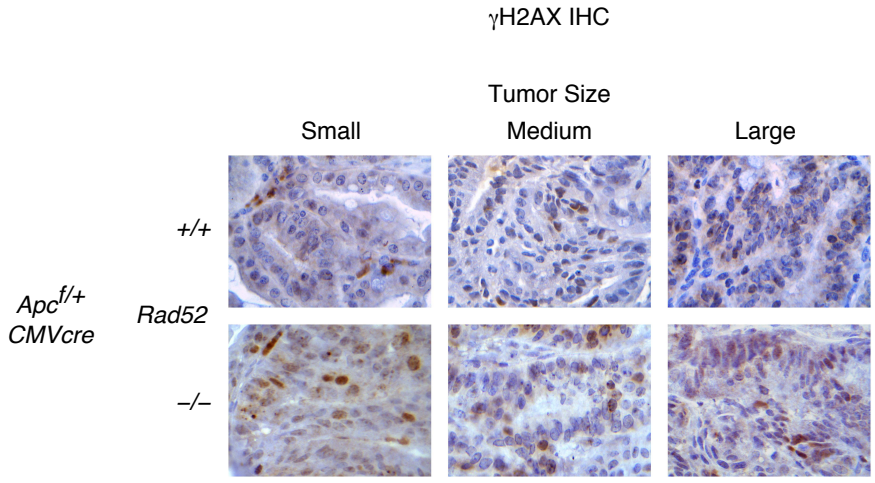

SUPPLEMENTAL FIGURE LEGENDS

Figure S1, related to Figure 1. Depletion or knockout of the *RAD52* gene targets preferentially cells with oncogene-induced DNA replication stress.

(A) EdU/BrdU profiles of cells treated with control (ctl) siRNA or siRNAs targeting *RAD52*, *MUS81*, *SMARCAL1* or *POLD4*, as determined by flow cytometry. The cells were treated as shown in Fig. 1A and the results obtained were used for the plots shown in Figs 1A and 1B.

(B) Sequences of the genomic loci targeted by CRISPR/Cas9 in three different clones of U2OS-Cyclin E cells. Two different mutant alleles were detected in clone 2G, whereas clones 3C and 4A harbored a single mutant allele. In clone 3C, a wild-type *RAD52* allele was also detected.

(C) Inactivation of the *RAD52* gene has small to modest effects on the static cell cycle profile of U2OS cells inducibly overexpressing cyclin E. The flow cytometry profiles of the three clones, in which the *RAD52* gene was targeted by CRISPR/Cas9, were compared to the profile of the parental cells (wt). The cells expressed normal levels of cyclin E (NE) or had cyclin E overexpressed (OE) for four days prior to the flow cytometry analysis. EdU was added to the media 1 hour before harvesting the cells. PI, propidium iodide.

(D) Means and standard deviations of the percentages of cells in the G1, S and G2 phases of the cell cycle, as determined by flow cytometry profiles, like the one shown in panel C (experiment performed in triplicate). One and two asterisks denote statistical significance levels of $P<0.05$ and $P<0.01$, respectively, and relevant statistical parameters are listed in Table S6.

(E) Deletion of the *RAD52* gene leads to reduced levels of DNA synthesis, as assessed by EdU incorporation. U2OS parental cells (wt) and clone 2G with both alleles of *RAD52* inactivated were labeled with EdU for 30 min and then examined by flow cytometry. The cells in G1 and S (colored red in the genomic DNA content versus EdU incorporation plots) were gated and the degree of DNA synthesis was monitored by histogram plots showing the levels of EdU incorporation. The histograms show overall higher levels of EdU incorporation in the parental cells, than in the 2G clone. PI, propidium iodide.

(F) Deletion of the *RAD52* gene slows progression through S phase and the cell cycle in general. U2OS parental cells (wt) and clone 2G with both alleles of *RAD52* inactivated were pulsed with EdU for 30 min and then cultured for an additional 12 hours, before being examined by flow cytometry. The EdU-positive cells were gated and genomic DNA content was monitored by histograms showing the levels of propidium iodide (PI) staining. The parental cells have higher peaks corresponding to G1 DNA content than clone 2G cells, indicating faster overall progression through the cell cycle. The G2 DNA content peaks of the wt cells are also better defined than the corresponding peaks of clone 2G cells, indicating faster progression through S phase.

Figure S2, related to Figure 2. Rad52 localization to sites of DNA replication stress.

(A) Representative immunofluorescence images showing colocalization of Rad52 and Atrip foci in cells overexpressing cyclin E (OE), as compared to cells expressing normal levels of cyclin E (NE).

(B) Representative immunofluorescence images showing partial colocalization of Rad52 and 53BP1 foci in cells treated with HU for 24 hours.

(C) Representative immunofluorescence images showing colocalization of Rad52 and RPA foci in cells treated with CPT for 24 hours.

Figure S3, related to Figure 3. Rad52 functions in repair of collapsed DNA replication forks.

(A) Collapse of DNA replication forks after treatment of U2OS cells with HU and a Cdc7 inhibitor for 24 hours. Cells were pulse-labeled with CldU for 40 min, then incubated with HU or HU plus a Cdc7 inhibitor (NMS-1116354) for 6 or 24 hours and finally pulse-labeled with IdU for 40 min in the presence or absence of the Cdc7 inhibitor, as indicated. Fork status was monitored by DNA fiber analysis. Re, restarted forks; Te, terminated forks; NF, newly-fired forks. The Cdc7 inhibitor inhibits new origin firing. This would include origins near collapsed forks, whose firing may be misinterpreted as fork restart.

(B) Efficiency of siRNA-mediated depletion of Rad52, Rad51, PolD3 and Mus81. Immunoblot analysis of Rad52, Rad51, PolD3 and Mus81 protein levels in U2OS cells 72 hours after siRNA transfection. α-actinin served as loading control.

(C) Scheme for synthesis of the Cdc7 inhibitor NMS-1116354. Synthesis of the inhibitor involved first the synthesis of two precursors: N-(2,2-dimethoxyethyl)acetamide (1) and ethyl 3-(2,4-dichlorophenyl)-3-oxopropanoate (2). The Cdc7 inhibitor (5-(2-aminopyrimidin-4-yl)-2-(2,4-dichlorophenyl)-1H-pyrrole-3-carboxamide) was then synthesized using the steps shown.

(D) Rad52 facilitates restart of collapsed DNA replication forks. U2OS parental cells (wt) and the *RAD52* knockout (KO) clone 2G were pulse-labeled for 1 hour with CldU followed by a 24 hour treatment with 2 mM HU and 5 μM Cdc7 inhibitor. The cells were then released from the HU block into media containing the Cdc7 inhibitor and IdU for 1 hour. Representative DNA fiber images, like the ones used to calculate the frequencies of fork restart in Fig. 3D are shown. CldU, red; IdU, green.

Figure S4, related to Figure 4. Immunohistochemistry for γH2AX in mouse intestinal tumors.

Representative immunohistochemistry (IHC) examples for γH2AX in small (diameter < 1.5 mm), medium (diameter 2-2.5 mm) and large (diameter 3-7 mm) tumors from *Rad52*$^{+/+}$*;Apc*$^{f/+}$*;CMVcre* and *Rad52*$^{-/-}$*;Apc*$^{f/+}$*;CMVcre* mice.

Table S1, related to Figure 1A.

Results of the low throughput siRNA screen performed in cells expressing normal levels of cyclin E (NE) or overexpressing cyclin E (OE).

For each siRNA or siRNA pool, the percentage of EdU-/BrdU- cells is indicated. Selected genes were targeted by more than one siRNAs or siRNA pools.

	EdU-/BrdU- (%)			EdU-/BrdU- (%)	
siRNA	**NE**	**OE**	**siRNA**	**NE**	**OE**
Control	36.7	11.2	RAD54L #1	42.6	14.0
53BP1	56.6	17.0	RAD54L #2	60.6	30.6
APEX2	38.1	18.6	RAD54L #3	56.0	19.8
ATRX	46.7	11.4	RAD54L2	32.4	12.3
BLM	43.1	5.9	RAP80 #1	44.8	14.3
BRCA2	42.8	12.9	RAP80 #2	32.8	16.7
DDX11	43.7	16.6	RDM1	35.1	13.0
DHX36	49.9	7.5	RECQL5	40.4	15.8
DNA2L	37.7	20.0	REV1L	44.3	10.4
DUT	42.7	12.3	RING1 #1	58.0	4.6
EME1	51.4	13.2	RING1 #2	64.6	30.7
EME2	42.3	5.4	RING1 #3	74.2	30.0
EXO1	68.6	19.1	RMI1	43.1	13.4
FAN1	76.1	35.2	RTEL1	67.6	18.4
GEN1	44.0	21.0	SFPQ	68.9	9.2
HELQ	38.2	16.9	SFR1	49.2	21.7
HELZ	41.4	11.4	SLX1	41.3	13.0
HLAB	42.7	12.8	SLX4	66.8	40.7
HORMAD1	41.3	13.5	SMARCA3	54.8	9.6
MCM8	24.0	11.3	SMARCAL1	42.0	29.2
MCM9	45.9	14.9	SMC5	28.9	5.5
MRE11A	44.2	16.9	SMC6	68.1	25.2
MUS81	49.0	35.3	SPATA5	32.3	12.7
NOXIN	42.3	12.2	SUB1	46.2	18.4
PIF1 #1	34.9	14.7	SWI5	38.8	9.3
PIF1 #2	38.2	13.0	SWS1	58.6	25.5
POLD2	46.2	15.2	SWSAP1	52.8	23.5
POLD4	45.9	29.3	TIMELESS	40.8	26.1
POLH	37.9	12.4	TIPIN	38.8	34.3
POLN	60.6	17.9	TONSL	51.4	20.9
POLQ	38.8	11.1	TREX2	60.0	28.8
RAD51	46.4	24.1	WDHD1	30.8	14.8
RAD51B	31.7	18.8	WRNIP1	53.1	15.9
RAD51C	29.5	9.2	XRCC2	39.2	20.9
RAD51D	43.8	22.4	XRCC3	33.2	15.5
RAD52 #1	58.1	33.2	ZRANB3	46.8	22.6
RAD52 #2	53.6	32.9			

Table S2, related to Figure 1.

Statistical analysis parameters. N1, N2, number of replicates/samples for the two groups being compared; df, degrees of freedom; P, level of statistical significance.

Fig 1B - % EdU-/BrdU- Cells					
Group Names	N1	N2	t test	df	P
OE cells: siControl vs siRAD52 #1	31	7	9.43	6.9	0.00004
OE cells: siControl vs siRAD52 #2	31	7	11.06	7.3	0.00001
OE cells: siControl vs siMUS81	31	6	15.65	7	0.00001
OE cells: siControl vs siSMARCAL1	31	7	14.59	10	0.00001
OE cells: siControl vs siPOLD4	31	5	6.36	4.4	0.003
OE cells: siControl vs siPIF1 #1	31	4	0.82	3.2	NS
OE cells: siControl vs siPIF1 #2	31	4	1.17	4.5	NS
NE cells: siControl vs siRAD52 #1	31	7	12.96	32.9	0.00001
NE cells: siControl vs siRAD52 #2	31	7	9	23.6	0.00001
NE cells: siControl vs siMUS81	31	6	4.2	8.9	0.002
NE cells: siControl vs siSMARCAL1	31	7	1.8	10.4	NS
NE cells: siControl vs siPOLD4	31	5	1.88	5	NS
NE cells: siControl vs siPIF1 #1	31	4	0.5	4.6	NS
NE cells: siControl vs siPIF1 #2	31	4	0.6	7.5	NS
Fig 1D - % EdU-/BrdU- Cells					
Group Names	N1	N2	t test	df	P
OE cells: RAD52 wt vs KO clone 2G	4	4	3.91	6	0.008
OE cells: RAD52 wt vs KO clone 3C	4	4	5.63	6	0.002
OE cells: RAD52 wt vs KO clone 4A	4	4	4.85	6	0.003
NE cells: RAD52 wt vs KO clone 2G	4	4	0.51	6	NS
NE cells: RAD52 wt vs KO clone 3C	4	4	4.7	6	0.004
NE cells: RAD52 wt vs KO clone 4A	4	4	5.57	6	0.002
Fig S1D - Cell Cycle Profile of Rad52 wt vs KO clones					
Group Names	N1	N2	t test	df	P
% Cells in G1: Cyclin E NE; Rad52 wt vs clone 2G	3	3	0.1	4	NS
% Cells in G1: Cyclin E NE; Rad52 wt vs clone 3C	3	3	3.1	4	0.04
% Cells in G1: Cyclin E NE; Rad52 wt vs clone 4A	3	3	1.7	4	NS
% Cells in G1: Cyclin E OE; Rad52 wt vs clone 2G	3	3	0.28	4	NS
% Cells in G1: Cyclin E OE; Rad52 wt vs clone 3C	3	3	0.18	4	NS
% Cells in G1: Cyclin E OE; Rad52 wt vs clone 4A	3	3	0.4	4	NS
% Cells in S: Cyclin E NE; Rad52 wt vs clone 2G	3	3	2.69	4	NS
% Cells in S: Cyclin E NE; Rad52 wt vs clone 3C	3	3	6.08	4	0.004
% Cells in S: Cyclin E NE; Rad52 wt vs clone 4A	3	3	5.68	4	0.005
% Cells in S: Cyclin E OE; Rad52 wt vs clone 2G	3	3	6.96	4	0.003
% Cells in S: Cyclin E OE; Rad52 wt vs clone 3C	3	3	2.86	4	0.05
% Cells in S: Cyclin E OE; Rad52 wt vs clone 4A	3	3	5.04	4	0.008
% Cells in G2: Cyclin E NE; Rad52 wt vs clone 2G	3	3	0.61	4	NS
% Cells in G2: Cyclin E NE; Rad52 wt vs clone 3C	3	3	0.21	4	NS
% Cells in G2: Cyclin E NE; Rad52 wt vs clone 4A	3	3	0.95	4	NS
% Cells in G2: Cyclin E OE; Rad52 wt vs clone 2G	3	3	1.75	4	NS
% Cells in G2: Cyclin E OE; Rad52 wt vs clone 3C	3	3	1.35	4	NS
% Cells in G2: Cyclin E OE; Rad52 wt vs clone 4A	3	3	1.98	4	NS

Table S3, related to Figure 2.

Statistical analysis parameters. N1, N2, number of replicates/samples for the two groups being compared; df, degrees of freedom; P, level of statistical significance.

Fig 2 - % cells with foci					
Group Names	N1	N2	t test	df	P
Fig. 2A: Rad52 foci NE vs OE	3	3	13.57	4	0.0002
Fig. 2A: RPA foci NE vs OE	3	3	3.34	4	0.03
Fig. 2A: Atrip foci NE vs OE	3	3	6.8	4	0.003
Fig. 2A: Rad51 foci NE vs OE	2	2	1.24	2	NS
Fig. 2C: Rad52 foci HU 0h vs 2h	3	3	4.54	4	0.02
Fig. 2C: Rad52 foci HU 0h vs 24h	3	3	7.82	4	0.002
Fig. 2C: RPA foci HU 0h vs 2h	3	3	2.2	4	NS
Fig. 2C: RPA foci HU 0h vs 24h	3	3	51.6	4	0.00001
Fig. 2C: 53BP1 foci HU 0h vs 2h	3	3	3.42	4	0.03
Fig. 2C: 53BP1 foci HU 0h vs 24h	3	3	7.88	4	0.002
Fig. 2C: Rad51 foci HU 0h vs 2h	3	3	0.27	4	NS
Fig. 2C: Rad51 foci HU 0h vs 24h	3	3	5.01	4	0.008
Fig. 2C: Rad52 foci CPT 0h vs 2h	2	2	4.57	2	0.05
Fig. 2C: Rad52 foci CPT 0h vs 24h	2	2	7.85	2	0.02
Fig. 2C: RPA foci CPT 0h vs 2h	2	2	26.8	2	0.002
Fig. 2C: RPA foci CPT 0h vs 24h	2	2	23.43	2	0.002
Fig. 2C: 53BP1 foci CPT 0h vs 2h	2	2	2.94	2	NS
Fig. 2C: 53BP1 foci CPT 0h vs 24h	2	2	6.47	2	0.03
Fig. 2C: Rad51 foci CPT 0h vs 2h	2	2	0.94	2	NS
Fig. 2C: Rad51 foci CPT 0h vs 24h	2	2	30.2	2	0.002

Table S4, related to Figures 3 and 4.

Statistical analysis parameters. N1, N2, number of replicates/samples for the two groups being compared; df, degrees of freedom; P, level of statistical significance.

Fig 3B - % cells in indicated γH2AX gate					
Group Names	N1	N2	t test	df	P
Medium (blue) γH2AX gate - 2h HU: siControl vs siRAD52	3	3	5.55	4	0.006
Medium (blue) γH2AX gate - 2h HU: siControl vs siPOLD3	3	3	1.25	4	NS
Medium (blue) γH2AX gate - 2h HU: siControl vs siMUS81	3	3	11.15	4	0.0004
Medium (blue) γH2AX gate - 2h HU: siControl vs siRAD51	3	3	22.19	4	0.00003
Medium (blue) γH2AX gate - 24h HU: siControl vs siMUS81	3	3	3.6	4	0.03
Medium (blue) γH2AX gate - 24h HU: siControl vs siRAD51	3	3	15.75	4	0.0001
High (red) γH2AX gate - 24h HU: siControl vs siRAD52	3	3	4.14	4	0.02
High (red) γH2AX gate - 24h HU: siControl vs siPOLD3	3	3	7.29	4	0.002
Fig 3C - % cells in high gH2AX gate					
Group Names	N1	N2	t test	df	P
High γH2AX gate - 24h HU: siControl vs siPOLD3	2	2	11.72	2	0.008
High γH2AX gate - 24h HU: siControl vs siRAD52	2	2	10.95	2	0.009
High γH2AX gate - 24h HU: siControl vs siPOLD3+siRAD52	2	2	25.13	2	0.002
High γH2AX gate - 24h HU: siRAD52 vs siPOLD3+siRAD52	2	2	0.52	2	NS
Fig 3D - Restarted Forks					
Group Names	N1	N2	t test	df	P
6h HU Rad52 wt vs KO clone 2G	3	2	5.72	3.5	0.007
24h HU Rad52 wt vs KO clone 2G	4	4	5.79	6	0.002
Fig 3E - BIR GFP Assay					
Group Names	N1	N2	t test	df	P
siControl vs siPOLD3	4	3	3.41	4.9	0.02
siControl vs siPOLD4	4	3	4.34	5.4	0.006
siControl vs siRAD52	4	3	8.53	4.8	0.0005
siControl vs siPOLD3+siRAD52	4	3	10.01	4.4	0.0004
siControl vs siPOLD4+siRAD52	4	3	6.36	6.9	0.0004
siRAD52 vs siPOLD3+siRAD52	3	3	2.42	4	NS
siRAD52 vs siPOLD4+siRAD52	3	3	1.21	4	NS
Fig 4A - Number of Tumors according to Size or Histology					
Group Names	N1	N2	chi square	df	P
Tumor Size: Rad52 +/+ vs -/- (all tumor sizes: 2x4 table)	46	50	11.73	3	0.009
Tumor Size: Rad52 +/+ vs -/- (tumor size: 0.5 mm: 2x2 table)	46	50	3.72	1	0.05
Tumor Size: Rad52 +/+ vs -/- (tumor size: 5-7 mm: 2x2 table)	46	50	9.38	1	0.003
Tumor Histology: Rad52 +/+ vs -/- (all histology types: 2x4 table)	46	50	3.13	3	NS
Fig 4B - Ki67 and γH2AX Indices					
Group Names	N1	N2	t test	df	P
Ki67 Index: Tumor Size 0.5-1.5 mm Rad52 +/+ vs -/-	9	14	0.13	22.4	NS
Ki67 Index: Tumor Size 2-2.5 mm Rad52 +/+ vs -/-	12	12	0.17	22	NS
Ki67 Index: Tumor Size 3-7 mm Rad52 +/+ vs -/-	24	16	1.66	27.6	NS
γH2AX Index: Tumor Size 0.5-1.5 mm Rad52 +/+ vs -/-	9	14	2.66	20	0.02
γH2AX Index: Tumor Size 2-2.5 mm Rad52 +/+ vs -/-	12	13	0.17	24.3	NS
γH2AX Index: Tumor Size 3-7 mm Rad52 +/+ vs -/-	24	17	0.75	36.5	NS
Fig 4C - Survival of APCmin Rad52+/+ and -/- Mice					
Group Names	N1	N2	z score		P
Rad52 +/+ vs -/- Mice	8	8	2.66		0.008

SUPPLEMENTAL EXPERIMENTAL PROCEDURES

Cell culture

U2OS cells expressing cyclin E in a tetracycline-dependent manner (U2OS-CycE) were cultured in Dulbecco's modified Eagle's medium (Invitrogen, 11960), supplemented with 10% fetal bovine serum (FBS) (Invitrogen, 10500), penicillin 100 U/ml and streptomycin 0.1 mg/ml (Invitrogen, 15140), G418 400 μg/ml (Invitrogen, 10131-027), puromycin 1 μg/ml (Sigma, P8833) and tetracycline 2 μg/ml (Sigma, T7660). To induce cyclin E overexpression, tetracycline was removed from the medium. U2OS cells were cultured in Dulbecco's modified Eagle's medium, supplemented with 10% fetal bovine serum (FBS).

siRNAs and plasmids

The following siRNAs were used: *RAD52*, GGAUGGUUCAUAUCAUGAATT (Qiagen, SI03035123) or GGUCCAUGCCUUUAAUGUUTT (Qiagen, SI03041808) or a pool of 4 siRNAs: ACGAAAACGCGUACUAAAA, GGCAUUAUGUCUAGGACUA, CAAUUA-GUGGUUAGGGAAA, UGUAUAGCAAGCUGAGUAA (Dharmacon, L-011760-00-0005); *SMARCAL1*, an equimolar mixture of two siRNAs: GCUUUGACCUUCUUAGCAA (Thermoscientific, J-013058-06-0005) and GCUUUGACCUUCUUAGCAATT (Qiagen, SI00103180); *MUS81*, UCUACCGGGAGCACCUGAAUCCUAA (Invitrogen, HSS129459); *POLD3*, a pool of 4 siRNAs: ACGAAAACGCGUACUAAAA, GGCAUUAUGUCUAGGACUA, CAAUUAGUGGUUAGGGAAA, UGUAUAGCAA-GCUGAGUAA (Dharmacon, L-026692-01-0005); *POLD4*, an equimolar mixture of two siRNAs: CACUAAUGCUUAUCAAUAATT (Qiagen, SI00688695) and CCCAUGAUCUGGCAAGUUATT (Qiagen, SI04189276) or a pool of 4 siRNAs: CCUAUGAGGCACCACGUAA, AGUCAGACAUGGACAGUUG, GGAUCAAG-UCCUCGGAAGA, CAAGAAAGUCCUAGGCCGA (Dharmacon, L-014013-02-0005); *RAD51*, GGGAAUUAGUGAAGCCAAATT (Qiagen, SI02663682); negative control, AllStars Negative Control siRNA (Qiagen, 1027281) or Luciferase GL2 (Invitrogen) or ON-TARGETplus non targeting pool siRNA (Dharmacon, D-001810-10-05). The pSpCas9(BB)-2A-GFP (PX458) expression vector was purchased from Addgene (#48138).

Flow cytometry screen

U2OS-CycE cells were plated in 6-well plates in the presence or absence of tetracycline and 24 hours later were transfected with siRNAs. The siRNAs were used at a final concentration of 10 to 50 nM and trasfected using either the Hiperfect reagent (Qiagen, 301707) or the Interferin reagent (Polyplus transfection, 409-50) according to the manufacturer's instructions. 72 hours later, the cells were treated for 1 hour with 10 μM EdU, then for 6 hours with 0.1 mM nocodazole and finally with 10 μM BrdU for 1 hour, before being harvested and fixed overnight at 4°C in 90% ice-cold methanol. The flow cytometry staining was performed as previously described (Costantino et al., 2014) with the following modifications: before staining with the anti-BrdU antibody (BD Biosciences, 555627), cells were blocked in PBS containing 1% BSA for 1 hour. Moreover, both the primary and the secondary antibodies were diluted in PBS containing 1% BSA.

Generation of U2OS-Cyclin E-RAD52 knockout cells

The pX458_Rad52_Crispr2 (Guide Sequence Insert: CACCGCCGGAGCTTCCGCTG-GTGCG) construct targeting exon 9 and the pX458_Rad52_Crispr6 construct (Guide Sequence Insert: CACCGTACATAAGTAGCCGCATGGC) targeting exon 3 of the human *RAD52* gene were designed and generated as described in the MIT CRISPR tool (Cong et al., 2013). U2OS-CycE cells were transfected with the 2 CRISPR/Cas9 constructs and GFP-

positive cells were sorted by FACS in 96-well plates. Single clones were expanded and genomic DNA extracted and used for PCR-based amplification of the targeted loci. For the targeted loci in exons 9 and 3, the CATCCGCCGTGGAGAGCGAGGCC and GGAACTGCTGCTGCAGCTGCTTC or the CCCTGAGGCAGAGGCTGGGCCCAG and CTCCTACCTTCTGGCCTCCGCC primers were used, respectively. Clones that appeared to have PCR products longer or shorter compared to the PCR product from the control wild-type cells were tested for Rad52 expression by western blotting. The genomic PCR products from clones with defective Rad52 expression were cloned into pCR-Blunt II-TOPO vector using the Zero Blunt TOPO PCR Cloning kit (Invitrogen, 450245) and analyzed by Sanger sequencing.

γH2AX detection by flow cytometry

For γH2AX detection by flow cytometry, U2OS cells were seeded in 6-well plates and the next day transfected with the indicated siRNAs at a final concentration of 40 nM using the Interferin reagent. 48 hours after siRNA transfection, the cells were treated with 2 mM HU for 0, 2 or 24 hours. The cells were then fixed with 70% ice-cold ethanol and left overnight at -20°C. The staining was performed using the FlowCellect Histone H2AX Phosphorylation Assay Kit (Millipore, FCCS100182) according to the manufacturer's instructions. The genomic DNA was stained by incubating the cells in PBS containing RNase (Roche, 11119915001) and propidium iodide (PI) (Sigma, P4170).

Immunofluorescence

U2OS-CycE cells were seeded on glass coverslips and 4 days after cyclin E overexpression were fixed in ice-cold methanol for 15 min at -20°C. U2OS cells were also treated for 0, 2 or 24 hours with 2 mM HU or 2 μM CPT and fixed. Cells were permeabilized in PBS containing 0.2% Triton X-100 (Sigma-Aldrich). The permeabilized cells were blocked with PBS containing 1% BSA and then were incubated with the corresponding primary antibodies (listed on the table below) for 2 hours at room temperature followed by 1 hour incubation with the secondary-antibody conjugates Alexa Fluor 488 (Thermo Fischer Scientific, A11001 or A11008) and Alexa Fluor 594 (Thermo Fischer Scientific, A11016). More than 80 cells per replicate and per condition were counted. The threshold to determine if a cell was positive for Rad52 foci was set at 20 foci per nucleus and for Rad51 at 10 foci per nucleus.

Preparation of Chromatin Extracts

U2OS cells were exposed to 2 mM HU for 24 hours or to 9 Gy ionizing radiation 1 hour prior to harvesting. Where indicated, the cells were exposed to HU in the presence of 10 μM ATR inhibitor (VE-821). For subcellular fractionation, the cells were harvested, incubated in Buffer A [8 μM Zinc Acetate, 10 mM Hepes pH 7.9, 1.5 mM $MgCl_2$, 10 mM KCl, 10 mM NaPO4 pH 8.0, and protease inhibitor cocktail (Roche, 05892970001)] for 10 min on ice and then centrifuged for 5 min at 1000 rpm at 4°C. The cells were resuspended in Buffer A, lysed using a Dounce glass homogenizer and centrifuged for 15 min at 3000 rpm at 4°C. The pellets were washed once more in Buffer A and centrifuged for 5 min at 1000 rpm at 4°C. Subsequently, the pellets were resuspended in Buffer B [8 μM Zinc Acetate, 20 mM Hepes pH 7.9, 1.5 mM $MgCl_2$, 300 mM KCl, 0.2 mM EDTA pH 8, 10 mM NaPO4 pH 8, and protease inhibitor cocktail], incubated for 1 hour on ice and centrifuged for 15 min at 3000 rpm at 4°C. The pellets, which correspond to the chromatin fraction, were resuspended in sonication buffer [50 mM Hepes pH 7.9, 140 mM NaCl, 1 mM EDTA, 1% Triton X-100, 0.1% Na deoxycolate, 0.1% SDS, protease inhibitor cocktail] and sonicated in a Bioruptor Pico sonicator (Diagenode). The samples were centrifuged for 15 min at 14000 rpm at 4°C and the supernatant which contained the chromatin fraction was collected and stored at -

20°C. For the phosphatase assay, the samples were treated as before but this time in buffers without EDTA and without phosphatase inhibitor cocktail. The samples were then treated with 800 units of λ-phosphatase, while in the control samples only the λ-phosphatase buffer was added without λ-phosphatase for 30 min at 30°C.

BIR-GFP reporter assay

U2OS cells with a stably integrated reporter construct for monitoring BIR were generated by transfecting the cells with the pBIR-GFP plasmid and then by selecting for stably-transfected clones (Costantino et al., 2014). The clone with the highest level of GFP induction after transfection with a plasmid expressing the I-SceI nuclease was selected for further experiments. In this clone, about 6% of the cells became GFP-positive, when I-SceI was expressed. For depletion of selected proteins, the following siRNAs were used: control, Dharmacon D-001810-10-05; *POLD3*, Dharmacon L-026692-01-0005; *POLD4*, Dharmacon L-014013-02-0005; *RAD52*, Dharmacon L-011760-00-0005. The cells were plated and two days later transfected with 20 ng of the indicated siRNAs and with 3 μg of the plasmid expressing I-SceI (pCMV-3xNLS-I-SceI) by Nucleofection using the Nucleofector Program X-01 (Amaxa-Lonza). Expression of GFP was monitored by flow cytometry 48 hours after transfection with the plasmid expressing I-SceI.

DNA fiber analysis

For the DNA fiber analysis, U2OS cells were pulse-labeled with 40 μM CldU for 40 min and then treated for 6 or 24 hours with 2 mM HU and with or without 5 μM Cdc7 inhibitor. Following the HU treatment, the cells were pulse-labeled with 400 μM IdU for 40 min or 1 hour in the presence or absence of 5 μM Cdc7 inhibitor. DNA fibers were prepared and stained as described previously (Ray Chaudhuri et al., 2012). Briefly, the cells were harvested, lysed and the DNA fibers were spread on APS-coated cover glass (Matsunami Trading, 7017.90000). The DNA fibers were denatured in 2.5 M HCl for 1 hour and blocked with PBS containing 0.2% Tween 20 and 2% BSA. The cover glasses were then incubated with primary antibodies against CldU (Abcam, ab6326) and IdU (BD Biosciences, 347580) for 2.5 hours. For visualization of CldU and IdU, the secondary antibodies Cy3 AffiniPure (Jackson ImmunoResearch, 712-166-153) and Alexa Fluor 488 (Thermo Fischer Scientific, A11001) were used, respectively. Finally, the fluorescence signal was amplified by using the secondary antibodies Dylight 550 conjugate (Thermo Fischer Scientific, SA5-10063) and the Alexa Fluor 488 (Thermo Fischer Scientific, A21467). More than 80 fibers per condition were counted.

Synthesis of the Cdc7 inhibitor

The synthesis strategy of the Cdc7 inhibitor (NMS-1116354; Montagnoli et al., 2010b) required a total of 8 steps including two steps for preparing precursors that are not commercially available (Fig. S5). The main steps were: i) the central aromatic pyrrole formation via a Knorr's reaction, ii) a regioselective electrophilic acylation, iii) the construction of the 2-amino-pyrimidine and iv) the primary amide formation. Except for the Knorr's reaction, which had a moderate yield of 34%, the yields of the other synthetic steps were good and reached at least 77%. The overall yield of the performed synthesis route was 17%. The identity and structural assignments of the intermediates and the final compound were assessed by ^{1}H-NMR, ^{13}C-NMR and LRMS. Spectral data were in total agreement with the structural formula of the synthesized compounds. Additionally, the identity and the quality of the final Cdc7 inhibitor were assessed by HRMS (HRMS (ESI+): expected m/z. 348.0413 for $C_{15}H_{11}N_5OCl_2$ [M+H]+; Found m/z: 348.0408) and High Performance Liquid Chromatography (purity >95%).

Mice

All mice were kept on a 12 hour light/dark cycle in an SPF room. The B6JIcoCrl.129P2-Rad52^{tm1Aps}/Cnrm mice were purchased from the European Mouse Mutant Archive (EMMA) (Rijkers et al., 1998). The C57BL/6-Apc^{tm1Tyj}/J mice were purchased from the Jackson Laboratory (Cheung et al., 2010). The CMVcre mice were obtained from the laboratory of Ivan Rodriguez at the University of Geneva (Dupe et al., 1997). The C57BL/6J-ApcMin/J mice were obtained from the laboratory of Joerg Huelsken at the University of Lausanne (Moser et al., 1990). Survival curves (euthanasia, as end-point) between Rad52$^{+/+}$;Apc$^{min/+}$ and Rad52$^{-/-}$;Apc$^{min/+}$ mice were analyzed in the Kaplan-Meier format using the log-rank (Mantel-Cox) test for statistical significance. All experiments involving mice were authorized by the Canton of Geneva and were performed according to accepted guidelines for animal handling.

Histological analysis

At the age of 8 months, Rad52$^{-/-}$;Apc$^{f/+}$;CMVcre and Rad52$^{+/+}$;Apc$^{f/+}$;CMVcre mice were euthanized according to approved animal protocols. The entire small intestine was rolled up into a "Swiss roll", fixed in formalin for 48 hours and embedded in paraffin for histological examination. A certified pathologist at the Medical School of the University of Athens performed the histopathological analysis.

Primary Antibodies used in this study

Antibody	Use	Dilution	Reference
α-Actinin	Western Blot	1/1000	Millipore, 05-384
H3 (phosphor T3)	Western Blot	1/5000	Abcam, ab78351
MCM5	Western Blot	1/500	Abcam, ab17967
MUS81	Western Blot	1/1000	Abcam, ab14387
POLD3	Western Blot	1/100	Abnova, H00010714-M01
RAD51	Western Blot	1/100	Santa Cruz, sc-8349
RAD52	Western Blot	1/200	Ochs et al., 2016
53BP1	Immunofluorescence	1/10	Schultz et al., 2000
ATRIP	Immunofluorescence	1/10	Venere et al., 2007
Cyclin E	Immunofluorescence/Western Blot	1/100	Novocastra, NCL-CYCLIN E
RAD51	Immunofluorescence	1/250	Abcam, ab63801
RAD51	Immunofluorescence	1/100	Santa Cruz, sc-8349
RAD52	Immunofluorescence	1/100	Ochs et al., 2016
RPA	Immunofluorescence	1/1000	GeneTex, GTX70258
γH2AX	Flow Cytometry	1/20	Millipore, CS208216
BrdU	Flow Cytometry	1/400	BD Biosciences, 555627
CldU	DNA Fiber Spreading	1/500	Abcam, ab6326
IdU	DNA Fiber Spreading	1/100	BD Biosciences, 347580
γH2AX	Immunohistochemistry	1/1000	Millipore, 05-636
Ki67	Immunohistochemistry	1/200	Abcam, ab16667

SUPPLEMENTAL REFERENCES

Cong, L., Ran, F.A., Cox, D., Lin, S., Barretto, R., Habib, N., Hsu, P.D., Wu, X., Jiang, W., Marraffini, L.A., *et al.* (2013). Multiplex genome engineering using CRISPR/Cas systems. Science *339*, 819-823.

Dupe, V., Davenne, M., Brocard, J., Dolle, P., Mark, M., Dierich, A., Chambon, P., and Rijli, F.M. (1997). In vivo functional analysis of the Hoxa-1 3' retinoic acid response element (3'RARE). Development *124*, 399-410.

Ray Chaudhuri, A., Hashimoto, Y., Herrador, R., Neelsen, K.J., Fachinetti, D., Bermejo, R., Cocito, A., Costanzo, V., and Lopes, M. (2012). Topoisomerase I poisoning results in PARP-mediated replication fork reversal. Nat. Struct. Mol. Biol. *19*, 417-423.

Schultz, L.B., Chehab, N.H., Malikzay, A., and Halazonetis, T.D. (2000). p53 binding protein 1 (53BP1) is an early participant in the cellular response to DNA double-strand breaks. J. Cell Biol. *151*, 1381-1390.

Venere, M., Snyder, A., Zgheib, O., and Halazonetis, T.D. (2007). Phosphorylation of ATR-interacting protein on Ser239 mediates an interaction with breast-ovarian cancer susceptibility 1 and checkpoint function. Cancer Res. *67*, 6100-6105.